Modelling Sea-Level Reconstructions from Southern Greenland: Implications for Glacially-Induced Faulting

by

Alexis Lepipas

A thesis submitted to the University of Ottawa in partial Fulfillment of the requirements for the Master's degree in Earth Sciences

Department of Earth and Environmental Science

University of Ottawa

Modelling Sea-Level Reconstructions from Southern Greenland: Implications for Glacially-Induced Faulting

by

Alexis Lepipas

Submitted to the Department of Earth and Environmental Science
on January 30, 2026, in partial fulfillment of the
requirements for the Master's degree
in Earth Sciences

Abstract

Understanding the past evolution of the Greenland ice sheet (GrIS) is important for accurately simulating its future behavior and thus its contribution to global mean sea level rise. Data and models related to glacial isostatic adjustment (GIA) have provided critical constraints on past GrIS evolution. These models are necessary to interpret a variety of data, including past sea-level changes and geodetic observations of current land motion and gravity changes. In all studies to date, paleo sea level data from southern Greenland have presented the greatest challenge to GIA models. Poor data-model fits in this region have led to the hypothesis of glacially-induced faulting during periods of rapid ice loss (with associated tsunami hazard).

In this study, we seek to determine if quality fits to the southern Greenland relative sea level (RSL) data can be obtained by improving the GIA model and exploring the parameter space more fully than past efforts. Specifically, we develop a revised ice sheet chronology for this region based on new data constraints, and we consider a small suite of 5 plausible global ice history models. We also consider the possible influence of lateral variations in earth viscosity structure via the use of a 3D (earth) GIA model. Our results show that RSL data at all sites (except Paamiut) can be fit well using our new deglaciation history, thus supporting this new model. Uncertainty associated with the input (global) ice model is large (up to ~20m) at some sites, and so should be considered when modelling RSL data in southern Greenland. The influence of lateral structure, while significant, is generally less than ~7m at most sites during the Holocene. The relatively poor fits at Paamiut are most likely related to inaccuracy in the local ice model and future work should explore this possibility. Overall, our results indicate that large magnitude faulting is not required to fit RSL data in southern Greenland.

Acknowledgements

I would like to begin by thanking my supervisor, Glenn Milne, for his patience in answering my questions and his thoughtful guidance throughout this work, always offering encouragement and support in a friendly and approachable manner. Through his supervision, I learned a great deal about sea-level research and geophysics, as well as gained valuable experience in professional development experience through workshops and conferences.

I would also like to thank my research group for teaching me new software, sharing codes and providing valuable support with GIA modelling. Especially, Parviz Ajourlou for his constant availability and introducing me to PyGMT plotting, and Ryan Love for his help with setting up ice sheet models.

J'aimerais également remercier mes parents, mes frères et mes amis pour leur soutien, tout au long de ce travail.

Table of Contents

Abstract ii

Acknowledgments iii

List of Figures vi

List of Tables viii

List of Abbreviations ix

Chapter 1: Introduction 1

1.1 Motivation and Aims 1

1.2 Relative sea-level change 2

1.2.1 Processes 2

1.2.2 Observations 3

1.3 Glacial Isostatic Adjustment 5

1.3.1 Overview 5

1.3.2 GIA modelling 7

1.3.2.1 Overview of Model Components 7

1.3.2.2 Determining the Ice History Model 8

1.3.2.3 Determining the Ice Earth Model 9

Chapter 2: Modelling Southern Greenland RSL 12

2.1 Introduction 12

2.2 Methods 14

2.2.1 RSL and Ice History Data 14

2.2.2 GIA Model 15

2.2.2.1 Overview 15

2.2.2.2 Ice History Models 16

2.2.2.3 Earth Viscosity Models 17

2.2.3 Data-Model Misfit Analysis 19

2.3 Results 19

2.3.1 Sensitivity Analysis 20

2.3.2 A Revised Ice Model Chronology for Southern Greenland..... 22

2.3.3 Identifying an Optimal 1D Earth Viscosity Model 24

2.3.4 3D Earth Modelling 28

2.4 Discussion 31

2.5 Conclusions..... 33

Chapter 3: Conclusion 35

References..... 38

Appendix 43

List of Figures

Figure 1-1 Diagram of isolation process and sample core of isolation basin 4

Figure 1-2 Types of RSL observations from southwest Greenland 5

Figure 1-3 Map of global ice extent at 19,000 years ago using HUY3 model..... 6

Figure 1-4 Schematic of the GIA process 7

Figure 1-5 Radial viscous structure of the spherically symmetric Earth models 10

Figure 1-6 Illustration on incorporating regional viscosity models into a global model . 11

Figure 2-1 Map showing the locations of RSL data and Be10 exposure ages in southern Greenland 14

Figure 2-2 Reconstructed RSL and exposure ages at all 5 sites in southern Greenland.. 15

Figure 2-3 Spatial extent of the disc applied to revise the HUY3 model ice history in southern Greenland 16

Figure 2-4 Depth slices of the log of viscosity variations inferred from lateral temperature variations..... 18

Figure 2-5 Contributions from different component signals to RSL at Nanortalik 20

Figure 2-6 RSL curves from all 5 global ice histories at Nanortalik 21

Figure 2-7 GMSL contributions from 5 different global ice histories 22

Figure 2-8 Ice thickness curves for HUY3 and HUY3 no YD GrIS histories 23

Figure 2-9 RSL curves for HUY3 and HUY3 no YD with the same earth model..... 24

Figure 2-10 Data-model misfit values in southern Greenland 25

Figure 2-11 RSL curves for the two earth model solution spaces determined from misfit calculations for three global ice sheet models 26

Figure 2-12 Data-model misfit values for all southern Greenland sites Paamiut..... 27

Figure 2-13 RSL curves for best two best scoring parameter sets..... 27

Figure 2-14 Modelled RSL with the addition of lateral viscosity in Greenland..... 29

Figure 2-15 RSL curves for 3D earth model versus the best scoring 1D earth model..... 30

Figure 2-16 RSL comparison of the 1D earth model and the 3D earth model..... 31

Figure 2-17 RSL comparison of the best parameter sets from this study and Lecavalier et al. 2014 32

Figure 3-1 RSL curves at Nanortalik for 15 GLAC3 Greenland ice models with the HUY3 (background) model 37

Figure S1 RSL curves for the 3D earth model and a closely related 1D earth model 43

Figure S2 Contributions from different component signals to RSL at 4 sites in southern Greenland for 14 – 0 ka 44

Figure S3 Contributions from different component signals to RSL at 4 sites in southern Greenland for 8 – 0 ka 45

Figure S4 RSL comparison for two different lithospheric thickness values 46

Figure S5 RSL curves for HUY3 no YD for different ε values 47

List of Tables

Table S1 **List of the subset of HUY3 and 15 GLAC3 ice models with their partnering 1D earth viscosity models.....48**

List of abbreviations

ANU	Australian National University (global ice sheet reconstruction)
GIA	Glacial Isostatic Adjustment
GLAC3-A/GLAC3-B	Variants of GLAC3 global ice sheet reconstructions (Lev Tarasov, personal communication)
GMSL	Global Mean Sea Level
GrIS	Greenland Ice Sheet
HUY3	Global ice sheet reconstruction from Lecavalier et al. (2014)
ICE-5G/ICE-6G	Global ice sheet reconstruction from Peltier et al. (2004) and Peltier et al. (2015)
LAB	Lithosphere-Asthenosphere Boundary
LGM	Last Glacial Maximum
LMV	Lower Mantle Viscosity
LP	Limiting Point
LT	Lithospheric Thickness
MLP	Marine Limiting Point
RSL	Relative Sea Level
Seakon	Finite-volume numerical GIA modelling software
SLIP	Sea-Level Index Point
TLP	Terrestrial Limiting Point
UMV	Upper Mantle Viscosity

Chapter 1: Introduction

1.1 Motivation and Aims

Coastal zones are becoming increasingly densely populated and are some of the most economically important regions on the planet. A human population of about 600 million is living in a low-elevation coastal zone (< 10m above sea level) (Hauer et al., 2021). As urbanization continues, historically unprecedented amounts of economic value of built infrastructure are being developed. It is estimated that the total cost of sea level rise in the 21st century - depending on the protection measures, retreat strategies and sea level rise rates - are projected to range between 2.5 trillion USD and 15.4 trillion USD (Ballesteros et al., 2025). These costs also include the contribution to an increased frequency of nuisance flooding and storm surge events, which have further amplified the social and economic challenges faced by lowland populations during the 21st century.

Among the contributors to global mean sea level (GMSL) rise, the Greenland ice sheet (GrIS) stands out as both a current and future threat. The volume of the GrIS represents approximately 7m of GMSL rise (Beckmann and Winkelmann, 2023) with melt rates already reaching 1mm/yr and expected to increase during the 21st century and beyond. In addition to the sea level impacts, melting of the GrIS also has the potential to weaken the Atlantic meridional overturing circulation (Van Westen et al., 2024). This change would result in warmer sea surface temperatures in the equatorial Atlantic and cooler values at the poles, which is projected to intensify storms and hurricanes in the north Atlantic and bring significantly colder winters to northwestern Europe (James Elsner, 2006; IPCC AR6 Chapter 9: Ocean, Cryosphere and Sea Level Change).

To better project the future trajectory of the GrIS and its regional to global impacts, it is important to understand its response to climate change on century to millennial time scales. The retreat of the ice sheet following the last glacial maximum (LGM) (~ 21,000 year ago) presents an ideal opportunity to quantify the sensitivity to the GrIS to climate warming and identify the underlying process. During the LGM the GrIS extended much farther onto the continental shelf and at its maximum extent at around 16,000 years ago, reached about 3 kilometers in thickness. However, the subsequent retreat of the GrIS has not been uniform in space nor time and so reconstructing this complex history requires the development and application of various paleo data sets and geophysical models. Paleo constraints such as relative sea level (RSL) data, ice cores or geomorphological evidence capture changes in local RSL, ice extent and ice surface elevation (amongst others). Models of glacial isostatic adjustment (GIA) are necessary to interpret past sea level changes in terms of local (Greenland) versus global changes in ice extent and to separate effects associated with ice evolution and solid-earth deformation. The complex

terrain and high precipitation in southern Greenland make the ice sheet more dynamic and thus responsive to climate change, thus highlighting the need to better understand the glacial history of this region.

Motivated by this issue, the work presented here will focus on improving paleo RSL data-model fits in southern Greenland during the last deglaciation. Despite the high quality of the RSL data in this part of Greenland, the quality of data-model fits in this region are some of the poorest in Greenland. The poor data-model fits have led to the hypothesis of large magnitude, glacially-induced faulting during a period of rapid ice loss around 10,500 years ago (Steffen et al., 2020). Using new developments in both ice sheet and GIA models, this thesis will assess whether the latest generation of models can accurately capture the observed RSL changes in southern Greenland without the need to induce large magnitude crustal faulting. Testing this hypothesis is particularly relevant in the context of large current and future rates of GrIS mass loss, which would increase the likelihood of future faulting events.

1.2 Relative Sea-Level Change

Sea level has been an important indicator for assessing changes in the global climate system as GMSL is an integrated measure of global warming/cooling. Sea level is, however, defined and measured locally via different methods. In this thesis, we define sea level as the height of the sea surface relative to the solid earth surface (ocean floor). This is a definition of RSL, which can be measured by tide gauges and geological proxies (Section 1.2.2).

1.2.1 Processes

Changes in RSL occur over several different spatiotemporal scales. Over relatively short periods of time (seconds to days) changes in sea surface height are mainly attributed to ocean-atmosphere interactions, tsunamis and tides. Over longer timescales (from centuries to millennia) three main processes influence RSL trends: (1) steric changes due to changes in ocean temperature and salinity as well as associated dynamic (ocean circulation) effects; the resulting changes in sea surface height are referred to sterodynamic sea level changes; (2) changes in continental ice distribution and associated changes to ocean volume, gravity and Earth's shape (i.e., through GIA) (see section 1.3); (3) tectonic processes influencing ocean floor height and gravity. All of these processes contribute to relative sea-level changes at local to global scales.

1.2.2 Observations

Modern day instrumental measurements of RSL obtained by tide gauges provide records spanning decadal to centurial time scales. However, constraints on longer time scales, which are the focus of this thesis, are generated from geological records. Describing methods used to reconstruct these geological records is the focus of this section. Past sea level reconstructions are derived from sea-level proxies, which are formed from sedimentary, geomorphic or biological indicators of the past position of sea level. Height and time constraints on past sea levels are defined by either sea-level index points (SLIPs) or limiting points (LPs). These points are characterized by a) geographic location (latitude and longitude); b) age determined by radiocarbon or U-Th dating; c) the altitude of the sample compared to contemporary sea level; d) how each proxy relates to mean sea level at the time it was formed called the "indicative meaning" (i.e., height the indicator formed within the local tidal range). Of course, there are uncertainties associated with all of these aspects of sea-level reconstruction. These are the four main criteria used to define paleo sea level data, but there are many other types of information that can be assigned (Khan et al., 2019).

To understand regional trends and departures from the global average, local paleo sea-level records such as SLIPs and LPs are essential. There are many types of proxies that can be used to generate SLIPs; among the most common in Greenland are isolation basins and salt marshes (Long et al., 2010; Long et al., 2011; Woodroffe., et al., 2014; Woodroffe et al., 2023). Isolation basins, are natural depressions that, initially, are below sea level and thus filled with marine sediments. As RSL falls due to GIA, the basin progressively becomes isolated from marine conditions and eventually becomes a freshwater basin (Figure 1.1).

Sediment cores from the basin are collected and analysed for microfossil content. The distribution of microfossils can be used to determine at what time the basin was isolated from the ocean, and the sill height defines the height of the highest astronomical tide at the age of isolation. This height and age pair defines the SLIP for that basin (Figure 1.2). While SLIPs indicate sea level at a specific time and elevation, not all sea-level proxies offer this level of precision.

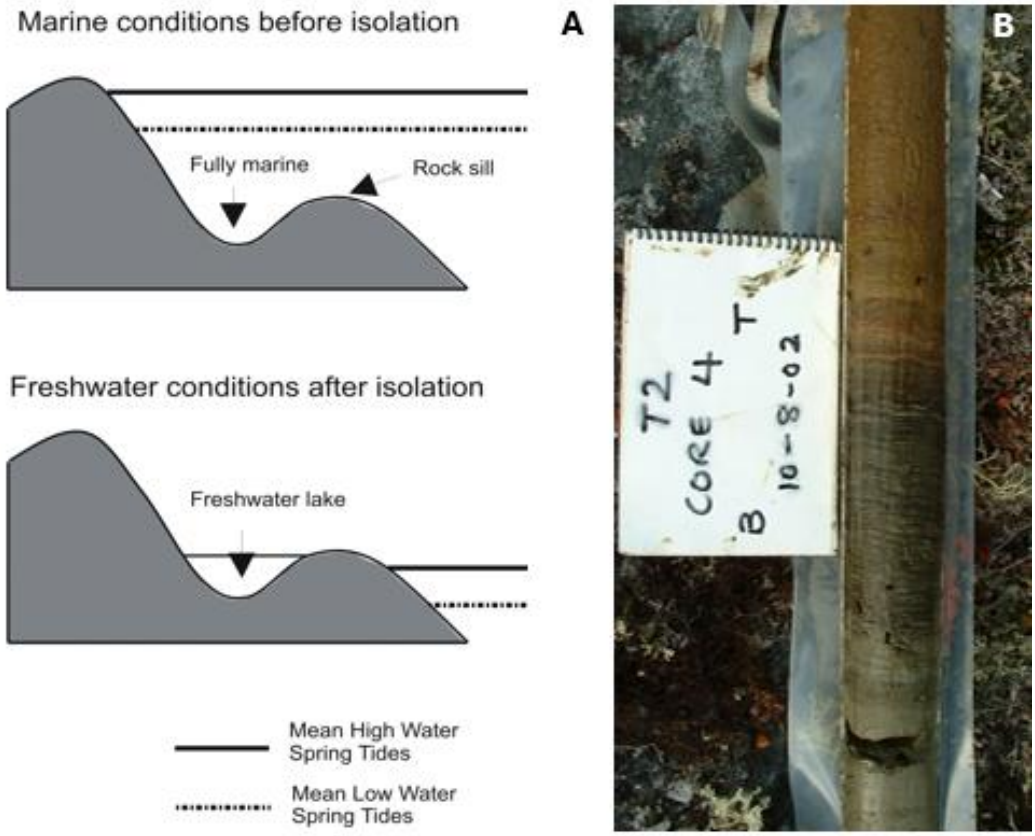

Figure 1.1. (A) Diagram showing the isolation process. (B) Sample core of an isolation basin shows the RSL record of an isolation basin. The light brown sediment in the upper (younger) part of the core was deposited in a freshwater environment. The darkest sediment was deposited in a brackish environment when the basin was below highest astronomical tide and thus partially marine. The oldest (gray) sedimentary layer is comprised of marine clays/silts and sands (Long et al., 2011).

In many cases, geological or biological indicators can only establish that sea level was either above or below a certain elevation. As previously mentioned, these are referred to as limiting points and are categorised as either marine limiting points (MLPs) or terrestrial limiting points (TLPs). Marine limiting points indicate that sea level was above the observed geological feature (e.g., marine sediment or deposit (Woodroffe and Long, 2010)), marine shells or mollusks (Long et al., 2011; Glueder et al., 2022), marine fossils (Bennike, 2000)). Meanwhile, terrestrial limiting points suggest that sea level was below the feature (e.g., archeological remains, terrestrial glacial deposits (Gowan, 2023) or beach deposits (Bennike and Weidick, 2007)). Among these limiting points, a key constraint is the marine limit, which defines the highest elevation at which marine conditions are evident after ice retreated. This upper limit on sea level can be a powerful constraint on GIA models. In Greenland, for instance, lakes with no marine sediments

or in-situ molluscs provide concrete evidence for marine limit elevation at a given location (Long et al., 2011; Glueder et al., 2022).

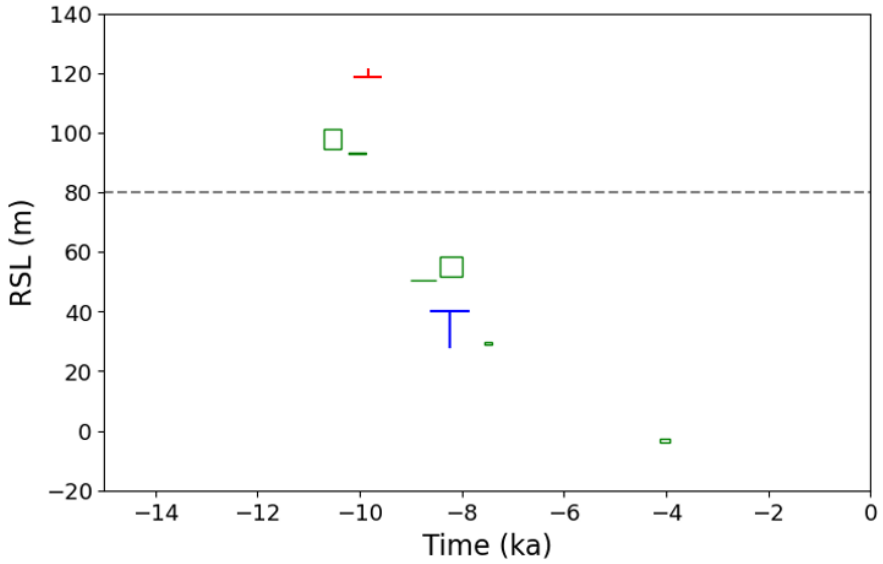

Figure 1.2. Plot of RSL observations from southwest Greenland, including sea level index points (SLIPs, green), marine limiting points (MLPs, blue), and terrestrial limiting points (TLPs, red). The marine limit is also shown (gray dashed line). Model prediction should intersect SLIPs, lie above MLPs, fall below TLPs, and should not exceed the marine limit once the region becomes ice free.

1.3 Glacial Isostatic Adjustment

1.3.1 Overview

GIA is the response of the Earth to changes in grounded ice extent. This response is characterised by solid earth deformations, changes in gravity and in the Earth's rotational state. While GIA studies can focus on any period of earth history when ice existed, most studies have considered the period following the LGM as the changes were large and the observational data sets are some of the best available. During the LGM (~25-19 ka), much of the Northern Hemisphere was covered by large ice sheets: most of Canada and the northern part of the United States were covered by the Laurentide ice sheet and the Eurasian ice sheet covered most of Fennoscandia, the British Isles and the Barents/Kara seas. During the LGM, the larger ice sheets exceeded 3,000 meters in thickness (Figure 1.3).

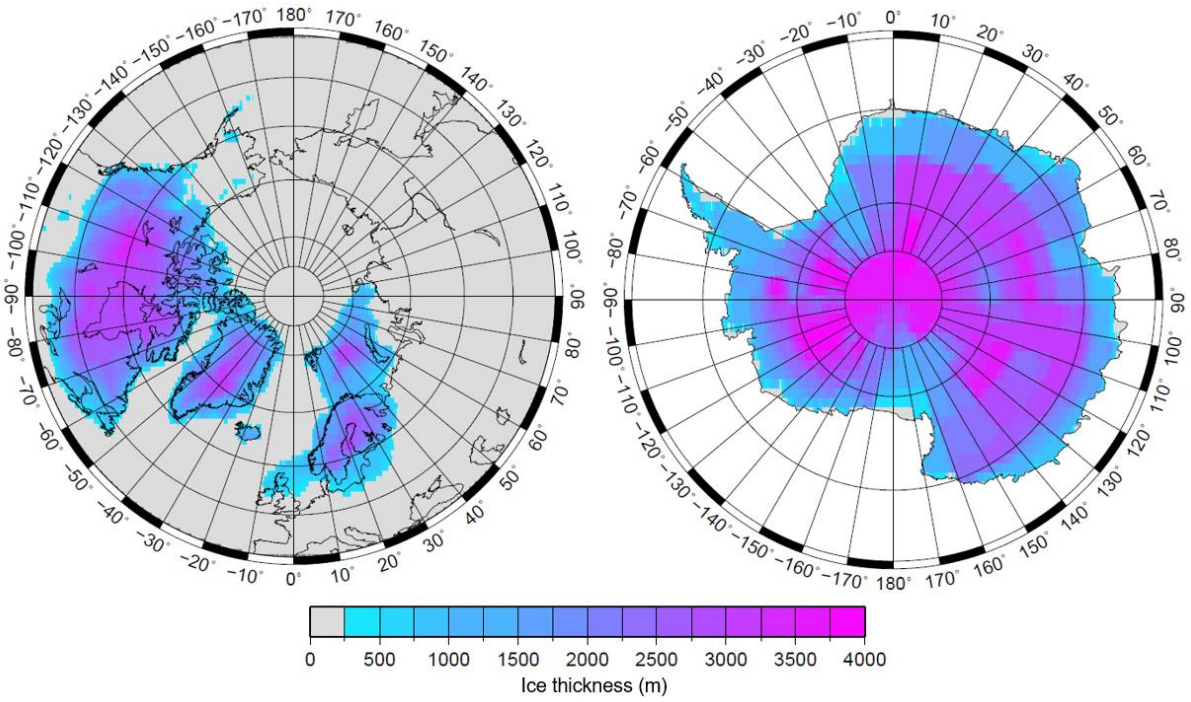

Figure 1.3. A global map of ice extent 19,000 years ago using the HUY3 model presented in Lecavalier et al. (2014).

Over millennial timescales, the gradual growth of the ice sheets prior to the LGM resulted in subsidence beneath the ice-covered regions through deformation of the lithosphere and mantle (Figure 1.4). As the lithosphere and mantle were compressed underneath the ice sheets, a subtle uplift is observed in regions peripheral to the ice associated with the elastic flexure of the lithosphere and flow within the sub-lithospheric mantle. As climate warmed following the LGM and the ice sheets began to melt this process is reversed: the peripheral areas subside and the solid Earth beneath the ice sheet begins to uplift (Whitehouse, 2018). This process is governed by the principle of isostasy which describes the response of the solid Earth to surface mass changes as it adjusts towards a new state of isostatic equilibrium. The geographic pattern and rate of isostatic adjustment depend on the rheological properties of the solid Earth as well as the surface loading changes in a given region. For instance, a region with a more viscous upper mantle layer will respond more slowly to surface loading or unloading compared to a region with a less viscous upper mantle (Milne and Shennan, 2013). The response amplitude depends on the magnitude of the surface load as well as earth rheology – particularly the elastic thickness of the lithosphere. A greater mass change and thinner lithosphere would result in a larger deformation.

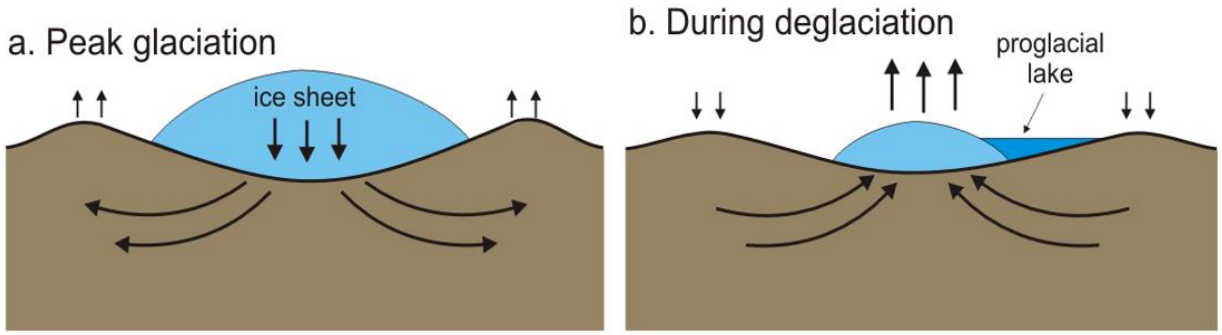

Figure 1.4. a) The lithosphere and mantle are compressed underneath the ice sheet causing subsidence beneath the ice sheet and uplift in the periphery of the ice sheet and in the direction of the arrows. b) When the ice sheet retreats due to climate warming, uplift occurs in ice-covered regions and subsidence occurs in peripheral regions. (Figure provided by Tom James, Natural Resources Canada).

The term GIA encompasses deformation associated with ice and ocean loading, and rotational changes. As previously mentioned, the ice sheet advances or retreats due to changes in climate. These changes in the ice sheet extent cause deformation of the solid earth. The deformational processes due to ice loading only are referred to as glacio-isostasy. Those related to the sea-level changes (ocean loading) associated with GIA are referred to as hydro-isostasy. In addition, to these loading effects, GIA encompasses the sea level changes associated with the changes in the volume of water in the global ocean. The contribution of this signal to GMSL change is termed barystatic sea level change. Finally, due to both forms of deformation and the redistribution of surface ice-water mass, the Earth's rotational potential is affected. This is also considered part of the GIA process as it results in gravitational changes and deformation (Milne and Shennan, 2013).

1.3.2 GIA Modelling

1.3.2.1 Overview of Model Components

A GIA model includes three elements: an ice loading history (Section 1.3.2.2), a model of earth rheology and density structure (1.3.2.3), and an algorithm to compute global sea level changes for a defined ice and earth model. This algorithm usually solves the so called "sea level equation" (Farell and Clark, 1976; Mitrovica and Milne, 2003).

Reconstructing the evolution of past ice sheets is necessary for modeling GIA and RSL change, as the chronology and extent of ice sheets directly influence relative sea level both globally, through meltwater and rotational contributions and locally, though solid Earth deformation (isostatic processes). Without well-constrained deglaciation histories, the Earth's response cannot be accurately modelled, therefore, constructing robust reconstructions of past ice extent and thickness is essential to producing

accurate GIA simulations (Section 1.3.2.2). Within the modelling framework, the ice sheet history is often varied to evaluate model sensitivity to alternative reconstructions and improve model accuracy.

A second key component is the Earth rheology and density model. This component is typically represented by either a spherically symmetric, Maxwell viscoelastic model or a more complex three-dimensional (3F) model which adds lateral variations to a chosen 1D (radial) viscosity profile (e.g., Ajourlou et al., 2025). Both of these model types will be applied in Chapter 2. As demonstrated in Chapter 2, variations in the viscoelastic structure of the earth model can result in large changes to the amplitude and rate of the isostatic response following ice retreat. The viscous component of this structure is often a free parameter in GIA modelling studies (e.g., Lecavalier et al., 2014). Further information on the earth model construction and parameterisation is provided in Section 1.3.2.3.

The sea level equation forms the mathematical core of GIA modelling as it includes the deformational changes of the solid Earth caused by changes in ice and ocean loads and the associated gravitational changes. This equation, originally presented by Farrell and Clark in 1976, allows us to calculate the global redistribution of meltwater across the oceans using the two key GIA model inputs models discussed above. It is important to note that the original sea-level equation (Clark et al., 1976) has been revised to include lateral variations in shoreline position and GIA-induced changes in earth rotation (Milne and Mitrovica 1998; Mitrovica and Milne, 2003) which is the version we will be using in this thesis.

1.3.2.2 Determining the Ice History Model

Ice history models can be developed using two complementary approaches: (1) via numerical (glaciological) models and (2) empirically using field data. The former approach involves numerical simulation of spatiotemporal ice evolution based on differential equations that represent the underlying ice physics. These simulations often require input information on the climate forcing (atmosphere and ocean) and the basal boundary conditions (e.g., isostatic response, heat flow, basal friction). The latter approach relies on geomorphological evidence such as moraines and other landforms, RSL indicators, climate proxies and geochronological data to date these proxies. Generally, empirical reconstructions provide high-resolution site-specific constraints. In contrast, modelling provides spatially consistent ice sheet evolution. Therefore, ideally, the two approaches are combined to validate simulations and estimate ice thickness across data-scarce regions.

In this thesis, we use several different ice history reconstructions that were produced using either a combination of the above two approaches or the empirical approach (combined with GIA modelling). Specifically, we use three ice model reconstructions that used glaciological modelling in parallel with the data constraints. These models are termed HUY3 (Lecavalier et al., 2014), GLAC3-A and GLAC3-B (Lev Tarasov, personal communication). The HUY3 model is a reconstruction of global ice extent over the past ~120,000 years. The Greenland and North American components were produced via glaciological modelling, with the Greenland component presented in Lecavalier et al. (2014) and the North American component presented in Tarasov et al. (2011). The other components of this global model (Eurasia, Antarctica, Iceland, Patagonia) were adopted from the ICE-5G model (Peltier, 2004) which was developed without the use of glaciological modelling. Further information on these different model components can be found in Lecavalier et al. (2014) and the references provided above for each component. The GLAC3-A and GLAC3-B models are global compilations of regional reconstructions, each of which was produced via data-constrained glaciological modelling (e.g., Lecavalier and Tarasov, 2025). We use two other global models in Chapter 2: a model developed by colleagues at the Australian National University (ANU; e.g., Lambeck et al., 2014) and ICE-6G (Peltier et al., 2015). These models were developed without the use of glaciological modelling and so are reliant on empirical constraints and GIA modelling (to constrain ice thickness).

The use of different ice sheet models is necessary to quantify the sensitivity of RSL in southern Greenland to the different model components. Past work has shown that GIA model output of RSL in Greenland is sensitive to both local (Greenland) ice and more distant ice sheets (e.g., Fleming and Lambeck, 2004; Simpson et al., 2009). This is due to the barystatic (meltwater) and associated hydro-isostatic contribution from all ice sheets but there is also a significant signal associated with gravitational and deformational (peripheral bulge) effects due to the North American and Eurasian ice sheets. By considering different ice sheet reconstructions (local to global) we are also able to quantify uncertainty associated with this primary GIA model input.

1.3.2.3 Determining the Earth Model

The solid Earth component of a GIA model is represented using either a spherically symmetric viscoelastic one-dimensional (1D) model (as introduced above) or a more complex three-dimensional (3D) model which adds lateral variations to a chosen 1D (radial) viscosity profile (Ajourlou et al., 2025). Both of these model types will be applied in Chapter 2.

For the spherically symmetric model, the internal structure consists of a relatively crude parameterisation of the viscous structure: an outer shell in which the viscosity is very large such that it simulates an elastic lithosphere (defined by its thickness), and a uniform viscosity in two underlying viscous layers representing the upper and lower mantle (Figure 1.4). This crude depth-parameterisation reflects our limited knowledge of the viscous structure and the relatively poor depth resolving power of GIA datasets. The elastic density structure is better known from seismic studies (Dziewonski and Anderson, 1981) and so these are defined with greater depth resolution (typically 1 km in the lithosphere and 10-50 km in the mantle). The three parameters defining the non-elastic component of the model earth response have a large influence on the amplitude and rate of modelled RSL changed.

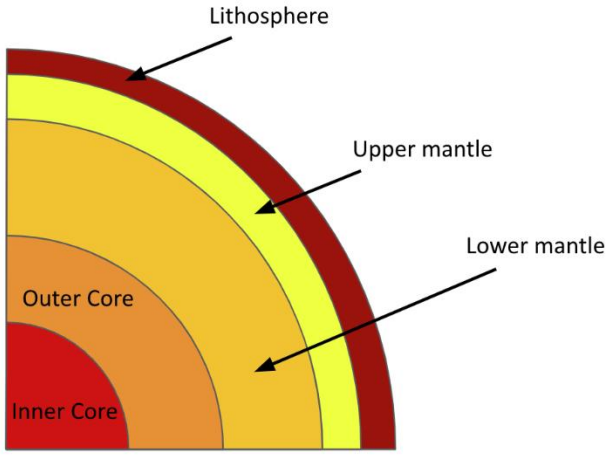

Figure 1.5. Radial viscous structure of the spherically symmetric Earth models used in this thesis.

We use the Seakon software (Latychev et al., 2005) to consider 3D earth structure in our GIA modelling. The first step in defining the 3D structure is to chose a reference radial (1D) model and then add lateral variations. The lateral structure is defined using constraints from seismic tomography. Specifically, we adopt a global shear wave velocity model and then determine the lateral viscosity by converting the velocity variations to viscosity variations via mineral physics constraints (Latychev er al., 2005; Milne et al., 2018). An important aspect of the 3D model used in Chapter 2 is that the lateral earth structure in the Greenland region is based on higher resolution, regional data sets (Ajourlou et al., 2025). This higher resolution regional model is patched into a global model (Figure 1.5). Due to the added structure, the more complex 3D model is computationally more expensive and so takes substantially longer to run than the simpler spherically symmetric model. Therefore, only a small subset of 3D model runs (<10) is presented in Chapter 2, compared to several thousand 1D model runs.

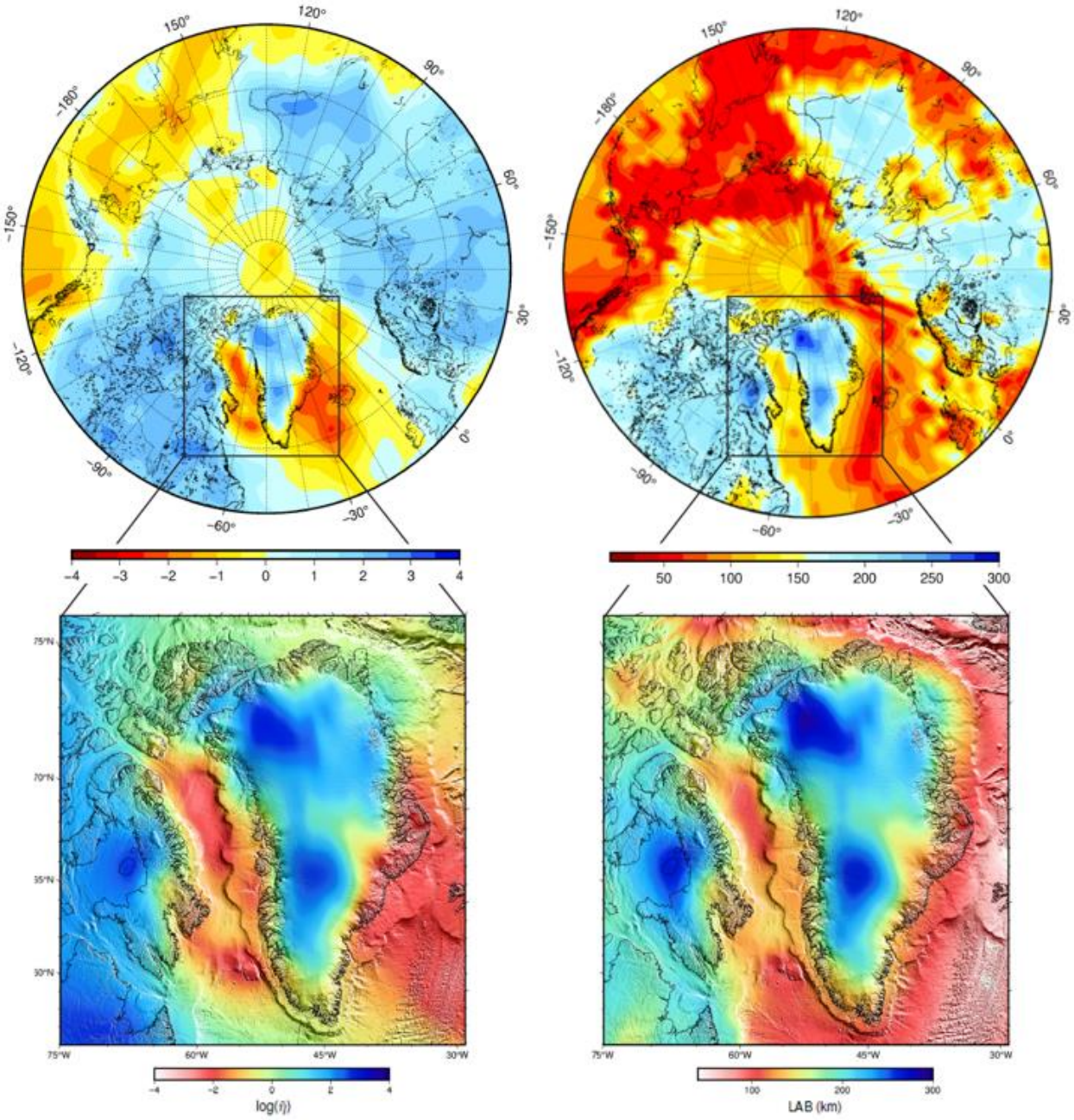

Figure 1.5. Incorporating regional viscosity models into a global model. Left: Lateral viscosity variations at depth 120km from the combination of regional and global viscosity models. Right: Lithospheric thickness from the combination of regional lithosphere asthenosphere boundary (LAB) model and a global model based on the results (from Ajourlou et al., 2025).

Chapter 2: Modelling Southern Greenland RSL

2.1 Introduction

Global mean sea level (GMSL) change is an important indicator for assessing changes in the global climate system as it provides an integrated measure of global warming/cooling. Among the contributors to global mean sea level (GMSL) rise, the Greenland ice sheet (GrIS) stands out as both a current and future threat. GrIS ice volume represents approximately 7m of barystatic sea level (Beckmann and Winkelmann, 2023) and the rate of melting is accelerating, with recent values exceeding 1 mm/yr (Otosaka et al., 2023). This sea level threat is paralleled by the influence of Greenland melting on weakening and potential shutdown of the Atlantic Meridional Ocean Circulation (Van Westen et al., 2024). Thus, there is a clear and urgent need to improve future projections of GrIS mass loss.

To better project the future trajectory of the GrIS and its global impacts, it is necessary to constrain and understand the response of the ice sheet to past changes in climate. However, the retreat of the GrIS since the last glacial maximum (LGM) has not been uniform in space or time and so reconstructing this complex history is difficult, due to the sparse distribution of observational constraints. The most useful constraints are generally obtained from reconstructions of ice extent (Funder et al., 2011; Sinclair et al., 2016; Levy et al., 2020; Funder et al., 2021; Leger et al., 2024) and relative sea level (Bennike and Weidick, 2007; Long et al., 2010; Long et al., 2011; Woodroffe et al., 2014; Nielsen, 2017; Glueder et al., 2022; Woodroffe et al., 2023; Gowan, 2023). They have been used to develop and test model reconstructions of GrIS evolution via glaciological and/or GIA modelling (e.g., Tarasov and Peltier, 2002; Fleming and Lambeck 2004; Simpson et al., 2009). The present extent of the ice sheet and geodetic observations of land motion and gravity are also useful constraints to test model accuracy (e.g., Simpson et al., 2011; Khan et al., 2016).

In the past ~15 years, there has been a dramatic increase in the amount and quality of these observational constraints. As a result, the more recently developed ice model reconstructions are constrained in most coastal areas around Greenland. For example, the model developed and presented by Lecavalier et al. (2014) provides quality fits to the RSL data in most areas. However, the model (termed HUY3) produced relatively poor fits in northwest and southern Greenland, primarily due to the magnitude of RSL fall being underpredicted (Woodroffe et al., 2014). Later work (Lecavalier et al., 2017) demonstrated that the poor fits in northwest Greenland are due to an inaccurate climate forcing for this region. The difficulty in fitting the amplitude of RSL data from southern Greenland have led to the hypothesis of glacially-induced faulting during periods of rapid ice loss (with associated tsunami hazard) (Steffen et al., 2020).

In past studies it has been suggested that adding lateral earth structure to Greenland GIA models will result in improved data-model fits (Simpson et al., 2009; Lecavalier et al., 2014). The first effort to address this task used constraints from global seismic tomography models to define 3D earth viscosity structure (Milne et al., 2018). The results show an increase in RSL amplitude relative to the spherically symmetric earth models, but the improvement is unable to match the observations. A more recently developed 3D model of earth viscosity structure, based on a joint inversion of regional data (Ajourlou et al., 2025) produce a greater RSL fall in southern Greenland and thus capture the data. However, the increased RSL amplitude leads to poorer data-model fits during the Holocene, suggesting that the regional HUY3 ice sheet reconstruction is inaccurate (Ajourlou et al., 2025). This is compatible with cosmogenic constraints relating to ice retreat in the area (Funder et al., 2021; Levy et al., 2020; Sinclair et al., 2016), which suggest an earlier retreat and a much reduced, or absent, readvance during the Younger Dryas.

In this chapter we seek to build upon previous studies by presenting new GIA model simulations for 5 sites in southern Greenland, with the aim of assessing whether high-quality fits can be obtained without including glacially induced faulting. This is achieved by: (1) performing a sensitivity analysis to identify the contributions from different component signals; (2) defining a suite of non-Greenland (background) ice models to explicitly include this source of model uncertainty; (3) defining a revised chronology for the southern GrIS that is more compatible with cosmogenic and RSL constraints; and (4) considering the influence of lateral variations in earth structure using a new 3D model determined from a recent joint inversion (Ajourlou et al., 2025).

2.2 Methods

2.2.1. RSL and Ice History Data

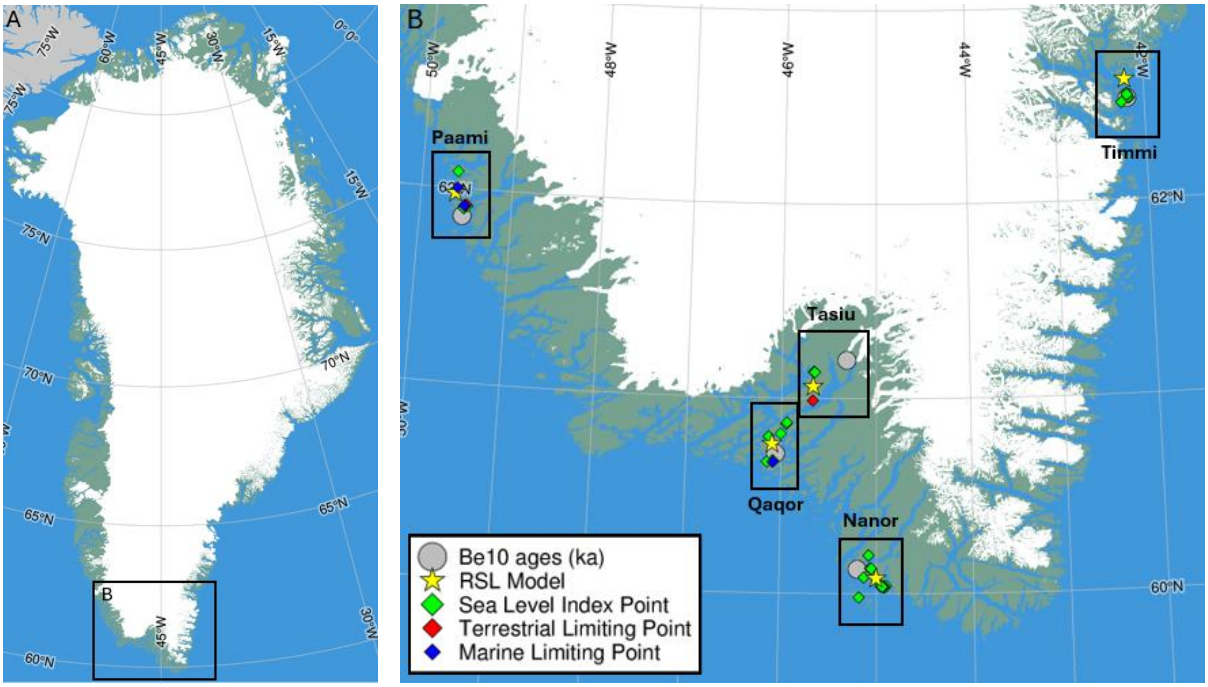

Figure 2.1. Map showing the locations of RSL data and Be10 exposure ages in southern Greenland. The data are grouped into 5 sites. (1) Paamiut (Paami), (2) Tasiusaq (Tasiu), (3) Qaqortoq (Qaqor), (4) Nanortalik (Nanor) and (5) Timmiarmiut (Timmi).

The RSL data used for this study are taken from Ajourlou et al. (2025). We have partitioned the data into 5 sites from southern Greenland (Figure 2.1). This dataset includes a total number of 53 RSL data points: 48 sea level index points (SLIPs), 3 marine limiting points (MLPs) and 2 terrestrial limiting points (TLPs) (Section 1.2.2). Hence, most of the data in the southern Greenland region are SLIPs which provide the most robust constraint on past RSL change (Figure 2.2). The south of Greenland includes a high density of SLIPs, contributing 39% of the Greenland wide number (48/123).

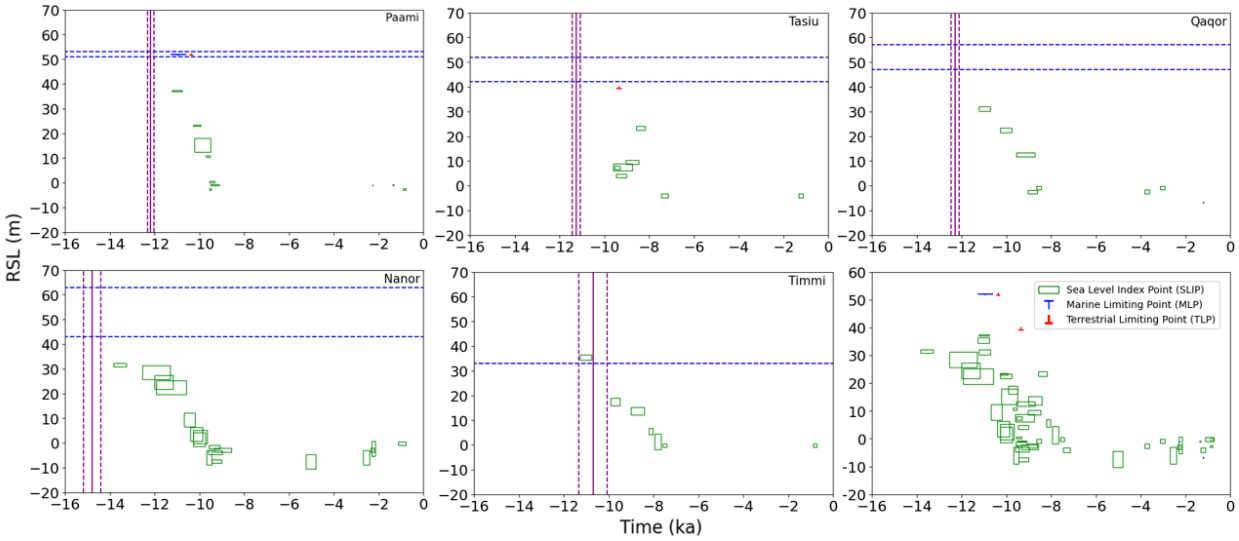

Figure 2.2. RSL reconstructions at all 5 sites considered. The vertical and horizontal dimensions of the SLIP boxes indicate the 2σ uncertainty in RSL and age, respectively. The bottom right plot represents all RSL reconstructions. Dashed blue horizontal lines indicate the marine limit (2σ uncertainty, Lutzenberg et al., 2026), and dashed purple vertical lines show uncertainty in the Be10 exposure ages.

RSL records consistently show a rapid fall during the early Holocene, generally between ~12–9 ka, though the timing can vary with location. At the southern tip, Nanor stands out by preserving the oldest RSL record and ice-free ages from cosmogenic data. Aside from this, the RSL records across all sites are broadly similar. Another notable difference is the more rapid rate of RSL fall at Paami and Tasiu. The ~25m SLIP at Tasiu is difficult to reconcile with the lower elevation SLIPs that pre-date it and some level of caution is reasonable regarding the accuracy of this data point. The westernmost site in the study region, Paamiut, displays a particularly rapid and pronounced RSL drop beginning at ~10.5 ka, the steepest of all five sites examined. Overall, the observed RSL trends align closely and thus support the accuracy of the reconstructions. The two data sets (exposure ages and RSL) are compatible since the oldest RSL data are the same age or younger than the Be10 ages. This compatibility gives confidence in the accuracy of these data sets.

2.2.2 GIA Model

2.2.2.1 Overview

Two different GIA models were used to compute sea level changes: (1) one that assumes a spherically symmetric (radial) Earth model and adopts the normal mode formalism for computing viscoelastic Love numbers (Peltier, 1974; Mitrovica and Peltier, 1991) and (2) one that considers 3D variations in global mantle viscosity structure and where the Earth deformation is computed numerically

via a finite volume approach (Latychev et al., 2005). Both models assume a compressible Maxwell rheology for the mantle and crust. The key inputs to each GIA model are (1) the earth model (section 2.2.2.3), and (2) the ice loading history (2.2.2.2). We computed RSL changes using the sea level equation described in Mitrovica and Milne, (2003), and the algorithm described in Kendal et al., (2005) with improvements to include GIA-induced changes in earth rotation (Milne and Mitrovica 1998; Mitrovica et al. 2005). We adopted a spherical harmonic truncation of 256, which provides spatial resolution of approximately 50 km in high latitude areas, such as Greenland. The 3D GIA model has a lateral grid resolution of ~20 km at the model-Earth surface and so has approximately twice the resolution as the radial model.

2.2.2.2 Ice History Models

We use ten ice history models in this analysis. All ice history models are defined with a temporal resolution of 500 years. These are comprised of two different models of ice thickness changes in southern Greenland and five different models for ice sheet changes beyond Greenland.

The two models for southern Greenland are the HUY3 model of Lecavalier et al. (2014) and a revised version of this model such that it deglaciates earlier. The revised chronology is integrated into the Greenland component by applying the revisions within a localized disc in southern Greenland (Fig 2.3), which ensures that the rest of the model ice history (in Greenland and beyond) is preserved (Fig 2.3). The revised HUY3 model is presented in Section 2.3.2.

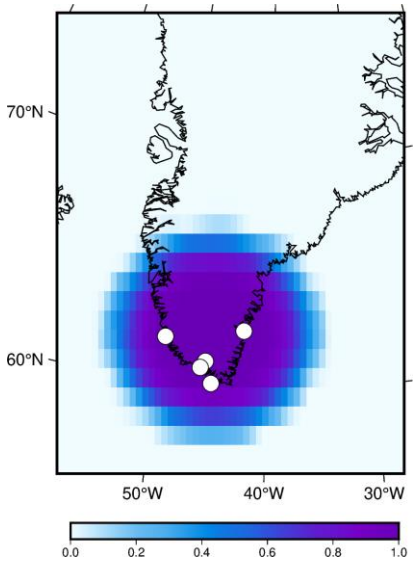

Figure 2.3. Spatial extent of the disc applied to revise the HUY3 model ice history in southern Greenland only. The applied mask tapers from a value of 1 to 0 around the margin of the disk to minimize edge effects.

The five different global (non-Greenland) models comprise: the Australian National University (ANU) reconstruction (Lambeck et al., 2014), ICE-6G (Peltier et al., 2015), HUY3 (Lecavalier et al., 2014) and two models produced by Lev Tarasov (personal communication). These models differ substantially in their distribution and timing of regional and global ice changes, allowing us to quantify the influence of individual ice sheet components on southern Greenland RSL. For instance, the ANU reconstruction includes a relatively thick Antarctic component and is the only model in our suite that features a 3-dome structure for the LIS. ICE-6G and HUY3 share broadly the same ice histories each having comparatively thin Antarctic component during the LGM. Finally, GLAC3-A and GLAC3-B have identical global models with the only difference being the Laurentide component. For example, GLAC3-A includes a larger NAIS (~78 m barystatic sea level) at LGM, compared to GLAC3-B (~72 m). These global models represent a high variance set and so provide a good representation of parametric uncertainty associated with this model input.

Merging regional ice sheet models into global reconstructions introduces challenges related to inconsistent spatial and temporal resolutions and overlapping ice sheet extents. For example, NAIS and GrIS models often overlap across the Canadian Arctic Archipelago. To address this, spatial masks were applied while merging to remove overlapping regions and to isolate contributions of individual regional ice sheets.

2.2.2.3 Earth Viscosity Models

The radial (1D) model is defined by three parameters: an outer shell with high viscosity emulating an elastic lithosphere, an upper mantle with uniform viscosity from the base of the lithosphere to the top of the lower mantle (670km), and a lower mantle which extends from the bottom of the upper mantle to the core-mantle boundary (2885km) which also has a uniform viscosity. These three parameters were varied across broad ranges to seek optimal fits to the RSL data. Specifically, lithospheric thickness (LT) values of 46, 71, 96, 120, 146 km were considered; 11 values for the upper mantle viscosity (UMV; 0.05,0.08,0.1,0.2,0.3,0.5, 0.8, 1,2,3,5 $\times 10^{21}$ Pas) and 10 for the (generally) more viscous lower mantle (LMV 1,2,3,5,10,20,30,50,60,90 $\times 10^{21}$ Pas). These parameter values result in a possible 550 Earth model parameter combinations. The elastic and density structure is more finely discretized and based on the seismic model PREM (Dziewonski and Anderson, 1981).

For the 3D Earth model, we adopt the optimum structure determined in a recent study that considered a Greenland-wide RSL data set (Ajourlou et al., 2025). The lateral component of this structure was determined via an inversion of multiple regional datasets to infer a 3D temperature model. These

temperature variations were then used to define lateral viscosity variations relative to a depth average value using the relationship,

$$\eta(r,\theta,\emptyset) = \eta_0(r)e^{-\epsilon\delta T(r,\theta,\emptyset)} \quad (2.1)$$

Where η_0 is the optimized radial viscosity model (LT = 71km, UMV and LMV = 10^{21} Pas), δT are the temperatures relative to a regional average, ϵ is a scaling factor and r, θ, and ∅ are the radius, colatitude, and east longitude. Figure 2.4 shows maps of this lateral structure at different depth slices. These results show surprising variations in viscosity across Greenland that are thought to be associated with the motion of the island over Iceland hotspot from about 90 to 20 Ma (Ajourlou et al., 2025). The viscosity values in southern Greenland tend to be low compared to the regional average, particularly for the upper few hundred kilometers. Given that there are considerable lateral variations in viscosity structure across Greenland, we developed a reference 1D viscosity model that closely matches the output from the optimal 3D model at Nanortalik (Fig. S1, Appendix). This 1D model includes the parameter values (LT = 90 km, UMV = 0.4×10^{21} Pas, LMV = 1×10^{21} Pas) and was used to perform the sensitivity analysis presented in Section 2.3.1.

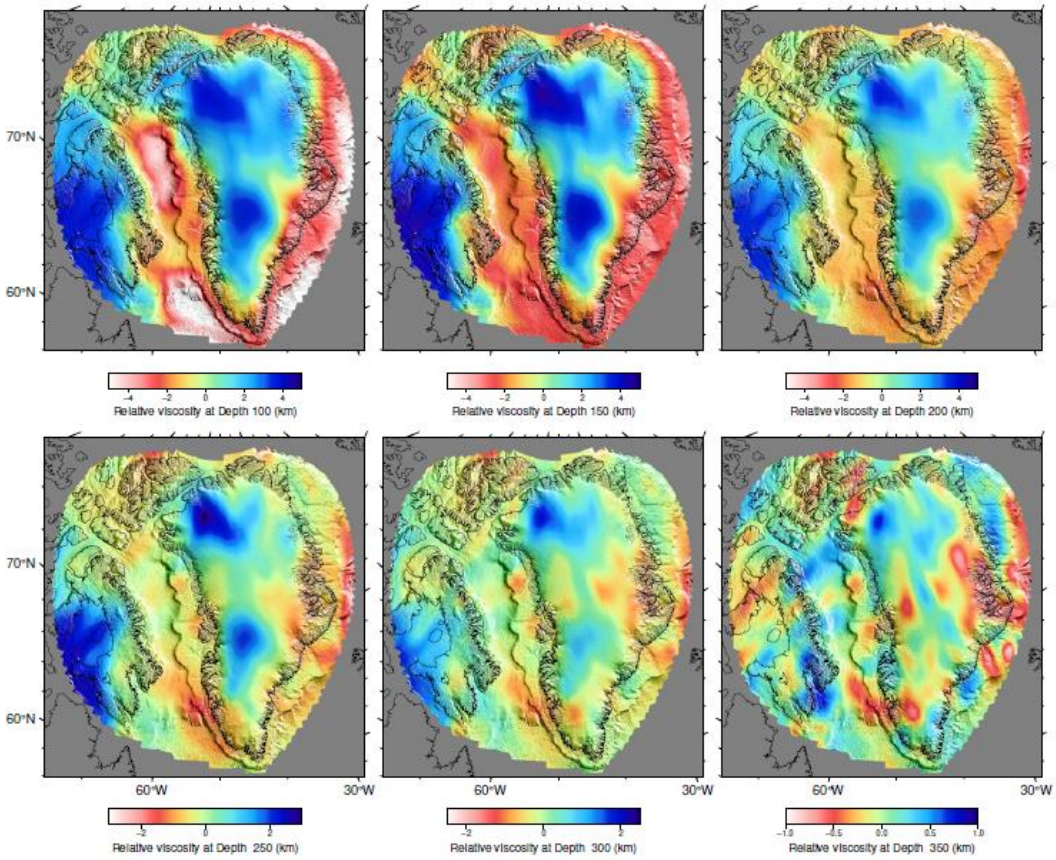

Figure 2.4. Depth slices of the log of viscosity variations relative to a defined reference value (η_0) via inferred lateral temperature variations and $\epsilon = 0.03°C^{-1}$in Eq. 2.1 (see Ajourlou et al. 2025).

2.2.3 Data-Model Misfit Analysis

The optimal parameter sets for the Earth model and ice loading histories are those that result in the lowest data-model misfit value. In computing misfit values, we follow the approach described in Parang et al. (2024), which is outlined in the following.

Due to the non-uniform distribution of RSL data points in space and time, spatio-temporal weighting was conducted on each RSL data type (SLIPs, MLPs and TLPs). For the case of SLIPs, the closest point on the model curve in height and time was determined and then the misfit value computed via

$$\delta_{SLIP} = \frac{\sqrt{\sum_{n=1}^{N}(\Delta_{RSL,n}^2/\sigma_{RSL,n}^2) + (\Delta_{t,n}^2/\sigma_{t,n}^2)}}{N} \quad (2.2)$$

Where $\Delta_{RSL,n}^2$ and $\Delta_{t,n}^2$ are the difference between observed and modeled RSL and age for a given observation, $\sigma_{RSL,n}^2$ and $\sigma_{t,n}^2$ are the given 2-σ observational uncertainty for the RSL and age of each observation, and N is the total number of observational data in southern Greenland.

Misfit values for limiting data were computed differently. If the model curve sat on the correct side of the limiting point (e.g., above a marine limiting point), no penalty was applied. However, if the model curve was on the wrong side of the point, a misfit was calculated via

$$\delta_{Lim} = \frac{\sqrt{\sum_{n=1}^{N}(\Delta_{RSL,n}^2/\sigma_{RSL,n}^2)}}{N} \quad (2.3)$$

This is due to limiting data provide only a one-sided height constraint on RSL. Since the limiting data provide only a one-sided constraint, they were weighted by 0.5 when calculating the total misfit.

$$\delta_{Total} = \delta_{SLIP} + 0.5\delta_{Lim} \quad (2.4)$$

2.3 Results

In Section 2.3.1 determine which component of the GIA signal (ice, ocean, rotation) affects the RSL signal the most and the effect of different global ice histories on southern Greenland RSL. We then create, in Section 2.3.2, a new chronology of ice deglaciation based on the HUY3 ice model. Using this new ice model we then compare RSL observations to model output to determine optimal (global) ice and earth model parameters using 1D earth models (Section 2.3.3). Finally, in Section 2.3.4 we evaluate the

impact of 3D earth structure on data-model fits to determine if this structure can significantly improve those obtained with the simpler 1D earth model.

2.3.1 Sensitivity Analysis

We partition the RSL signal in southern Greenland into the components associated with ice loading, ocean forcing, rotational effects and GMSL (which includes barystatic and syphoning signals). The contributions of these components are evaluated to determine their relative influence on RSL for the time interval data are available. These sensitivity tests will be, useful when deciding upon the model parameter suite to consider for the forward modelling analysis and when interpreting the results of this analysis. Figure 2.5 shows that the ice-induced signal and GMSL are the largest contributors, but with opposite sign, throughout most of the deglacial period. Since the positive ice-driven signal is larger than the GMSL signal, there is a moderate fall in RSL overall.

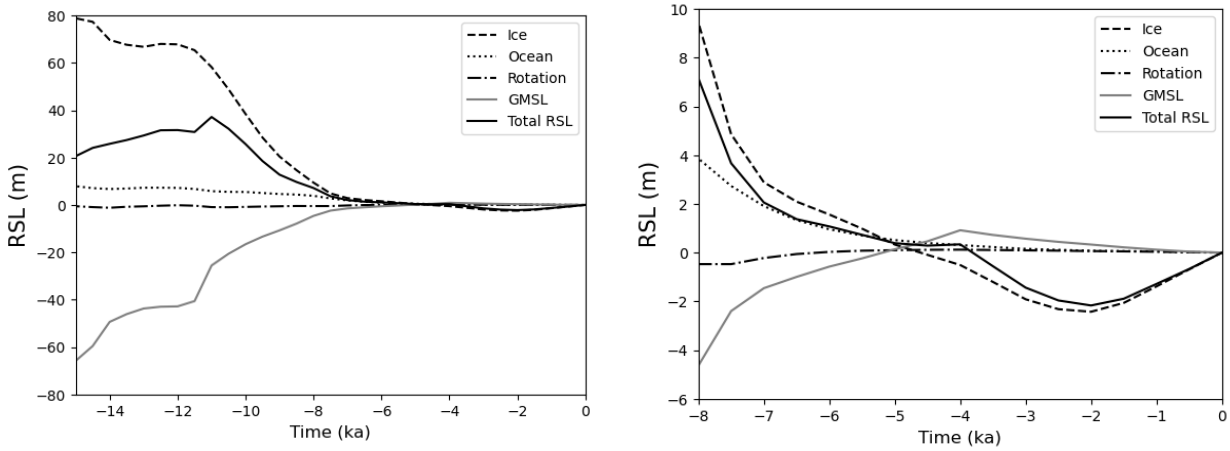

Figure 2.5. Contributions from different component signals (see key) to RSL at Nanortalik. Results are based on the HUY3 ice model and earth model parameters LT = 90 km, UMV = 0.4×10^{21} Pas, LMV = 1×10^{21} Pas. Results for the other four sites considered are shown in Fig.S2 (Appendix) for 0 – 14 ka and Fig.S3 (Appendix) for 0 – 8 ka.

The ice-induced RSL fall is dominated by land uplift in response to ice loss in southern Greenland. From ~14ka through to the early Holocene (~10 ka), the total RSL signal rises steadily due to the dominance of GMSL change associated with the rapid melting of global ice sheets in North America, Scandinavia and Antarctica. This RSL rise sharply transitions into a RSL fall at the onset of rapid thinning in the HUY3 model around 11 ka, after which the ice-induced signal dominates. The combined effects of regional uplift and rising GMSL brings the total RSL to within a few meters of its present-day value by approximately 7 ka. After 2-3 ka the dominant effect becomes subsidence in the region associated with

the peripheral bulge causing RSL to rise (Lecavalier et al., 2014; Simpson et al., 2009). The results in Fig 2.5 demonstrate the importance of both the global and local ice-induced signals.

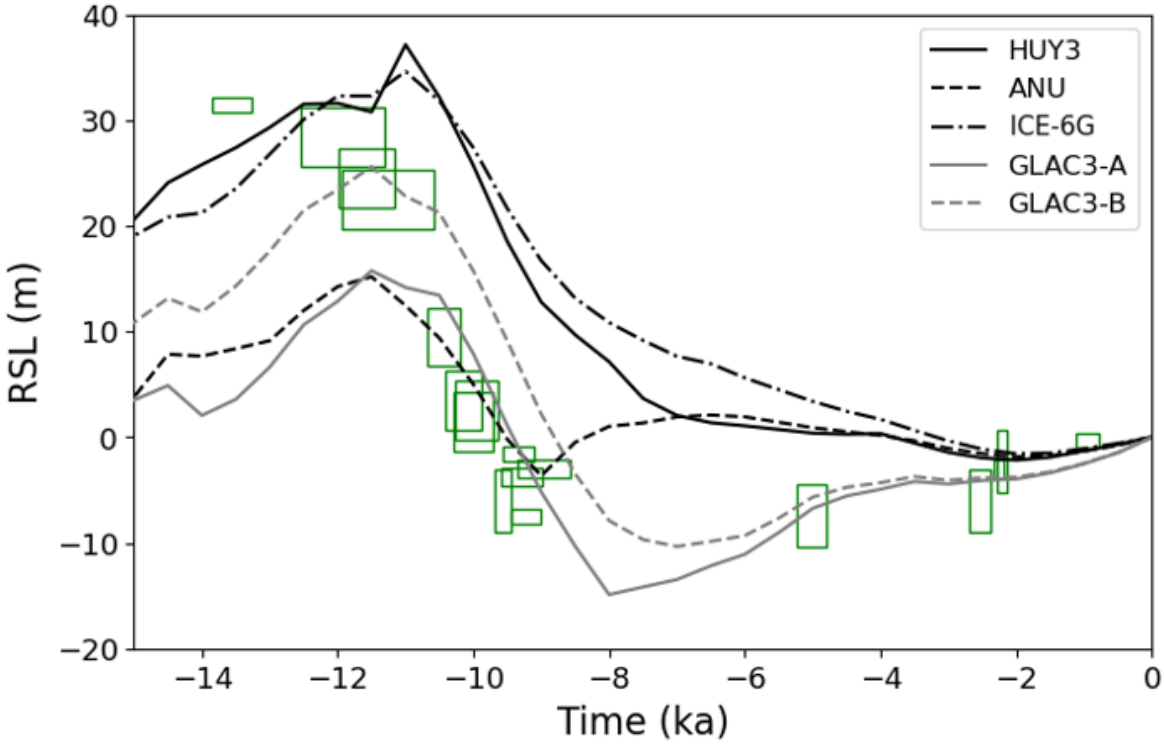

Figure 2.6. RSL curves from HUY3, ANU, ICE-6G, GLAC3-A and GLAC3-B at Nanortalik. All models use the same local Greenland ice model (HUY3) to isolate the RSL differences associated with choosing different global ice reconstructions. The green squares are reconstructed RSL (SLIPs) at this site.

To determine the influence of uncertainty in the input global ice sheet history, we conduct a sensitivity analysis using 5 different global ice model reconstructions. Figure 2.6 demonstrates that the non-local ice signal alone can produce substantial variability in southern Greenland RSL, with differences of exceeding 20 m. These variations are primarily driven by differences in volumes of the NAIS and AIS components of these model reconstructions. This is reflected in Fig 2.7 which shows the GMSL contribution for each of the different global models considered. Differences associated with the NAIS component of the ice model are isolated by comparing results for the two GLAC3 models, which share identical global ice components except for the NAIS. GLAC3-A includes a larger NAIS component, contributing approximately 78m of barystatic sea level, whereas GLAC3-B has a smaller contribution of about 72m. The differences shown between these model curves in Fig 2.6 (grey solid and dashed lines) are dominated by the different barystatic signal (Fig 2.7) and the influence of different NAIS components on the ice-induced signal (particularly that associated with the peripheral bulge and gravitational effects). The difference between these two model curves from ~7 ka to present is due to the bulge effect only as

the other signals are close to zero over this period. The differences in the NAIS component of the two GLAC3 models lead to a ~10 m difference in RSL at Nanortalik, or ~30% of the observed RSL variation.

The results in Figs 2.6 and 2.7 demonstrate that the uncertainty in ice sheet changes beyond Greenland have a significant influence on RSL changes in southern Greenland and so must be considered when seeking optimal earth and/or ice model parameters from RSL data. Assuming our earth viscosity model is relatively accurate, the results also indicate that ice reconstructions with smaller NAIS and AIS components provide better agreement with the observed RSL amplitudes, as evident for HUY3 and ICE-6G. However, HUY3 and ICE-6G perform more poorly at capturing SLIPs below 10 m elevation. This suggests that revisions to the local (GrIS) reconstruction are necessary to better capture the amplitude and timing of the reconstructed RSL variations.

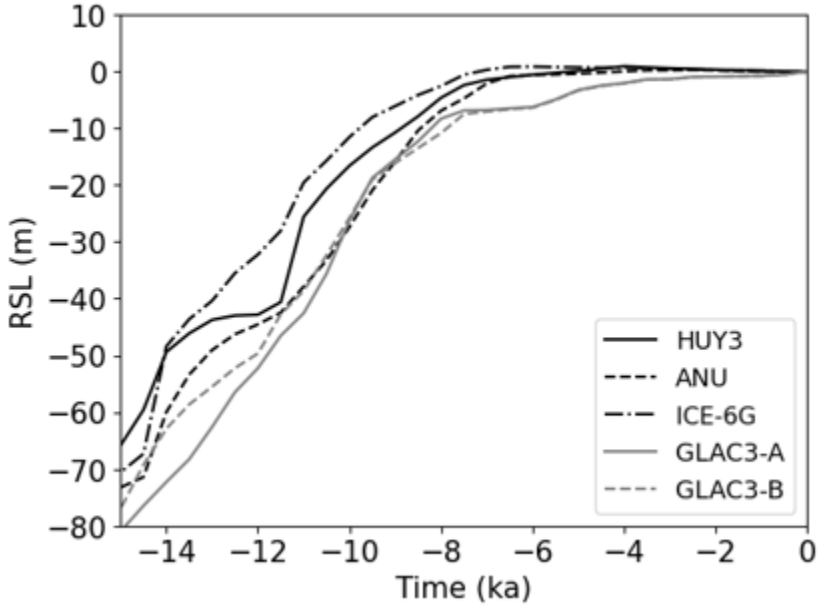

Figure 2.7. GMSL contribution from 5 different ice sheet models with the same GrIS component (HUY3) but different global components (see key).

2.3.2 A Revised Ice Model Chronology for Southern Greenland

In this section, we revise the local ice model chronology such that it is more compatible with the Be-10 constraints and the RSL data (Section 2.2.1). As noted above, models that better capture the amplitude of the RSL variation generally produce a RSL fall that is delayed compared to the observations. This is consistent with the timing of ice-free conditions in the HUY3 ice model being significantly later than indicated by the cosmogenic data (Figure 2.8). The late timing of modelled ice-free conditions is also inconsistent with the RSL observations, as the geological records used to reconstruct these data can only

be generated once the locality is ice free. This aspect has not been given sufficient attention in previous studies (e.g., Lecavalier et al., 2014).

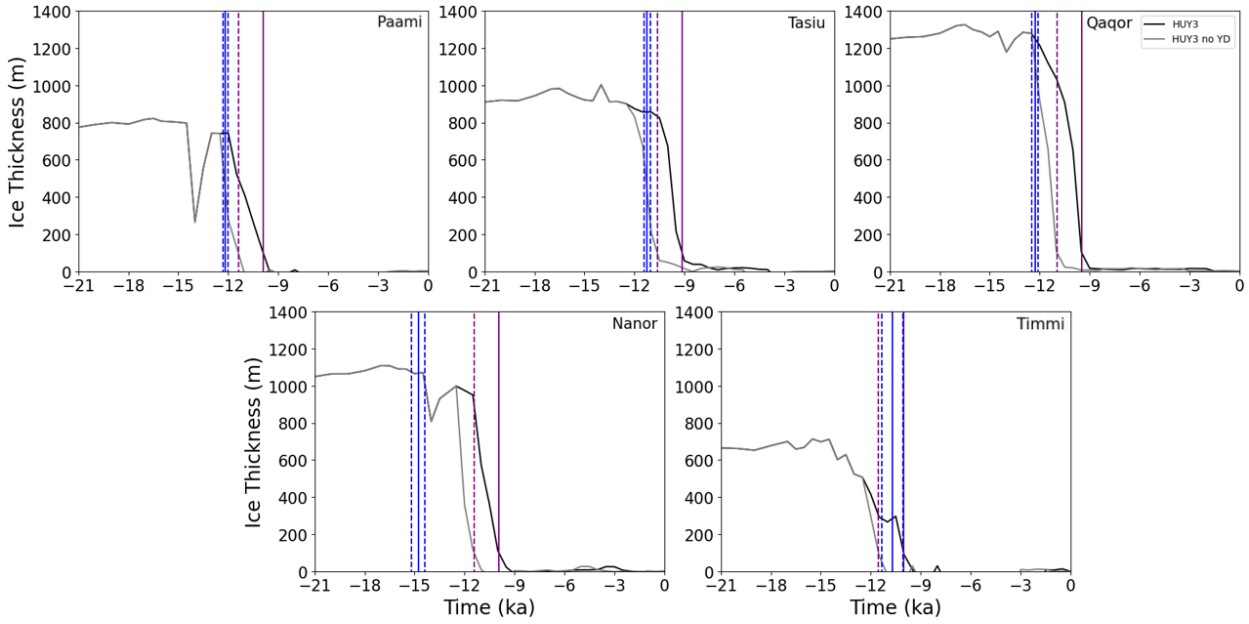

Figure 2.8. Ice thickness at all 5 sites using HUY3 (black line) and HUY3 without a Younger Dryas (YD) readvance (gray line) GrIS components. The solid blue vertical line show exposure ages (Levy et al., 2020) and the dashed blue vertical lines show the uncertainty in exposure ages, while the purple vertical line shows modelled ice-free conditions (when ice thickness is below 100 m) for the HUY3 (solid lines) and HUY3 no YD (dashed lines) model.

As described in Section 2.2.2.2, we isolated the southern Greenland component of the HUY3 model using the spatial function shown in Fig. 2.3. We then considered several different variations of the ice chronology in this region such that the timing of ice free conditions are more compatible with the cosmogenic constraints and the RSL observations. This exercise proved difficult because satisfying the cosmogenic data resulted in poorer fits to the RSL data, and vice-versa. The model we chose represents a deglaciation scenario that provides a 'middle ground' in the sense that ice free conditions occur late relative to the cosmogenic data (Fig. 2.8) but the modelled RSL fall is early relative to the sea-level reconstructions (Fig. 2.9). The revised ice model will be referred to as "HUY3 no YD" since it was created by effectively removing the Younger Dryas readvance in the original HUY3 model. In the next section, we seek an optimal fit to the RSL data using this new ice model for southern Greenland.

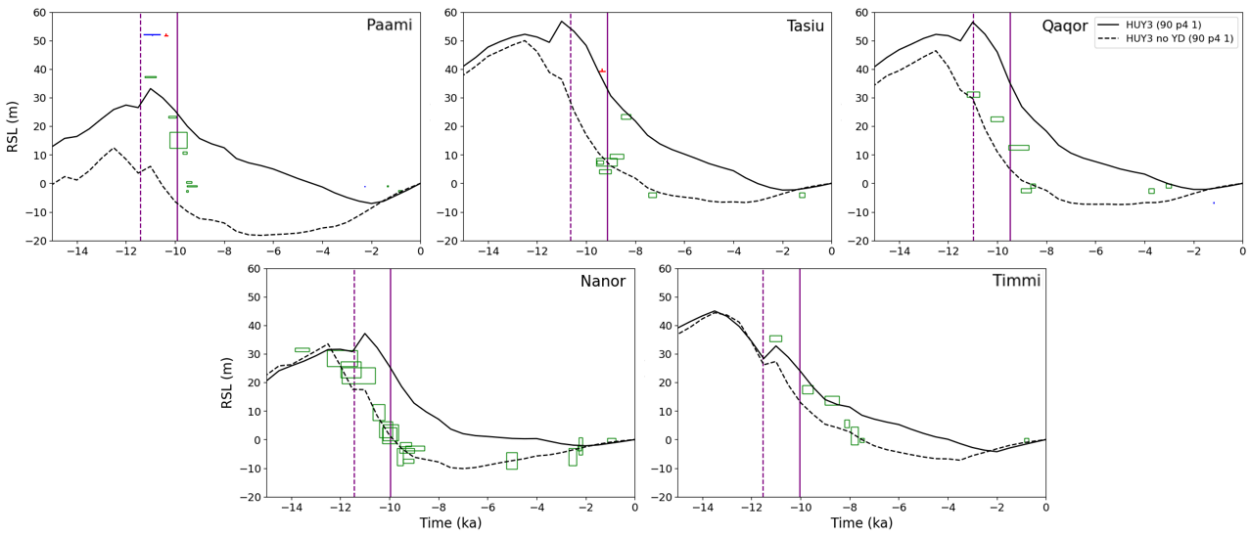

Figure 2.9. RSL curves using the HUY3 (solid black line) and HUY3 no YD (dashed black line) ice sheet models with an earth model of LT = 90 km, UMV = 0.04×10^{21} Pas, LMV = 1×10^{21} Pas. The solid purple vertical lines show modelled ice-free conditions (when ice thickness is below 100 m) for the HUY3 (solid) and HUY3 no YD models (dashed).

2.3.3 Identifying an Optimal 1D Earth Viscosity Model

We present the data-model misfit calculations for the revised southern Greenland chronology identified in the previous section. We consider 5 global ice model reconstructions and 550 earth models (i.e., a total of 2750 simulations). The misfit results (Fig 2.10) indicate significant sensitivity to changes in the non-Greenland ice model (compare results in each row). Therefore, as is common in GIA problems, there will be a degree of non-uniqueness in defining which parameter sets offer the optimal data model fits. Generally, when considering results for all data (first row in Fig 2.10), two distinct viscosity model solution spaces are observed which provide low misfit values. The first is characterized by Earth models with relatively low UMV (0.05×10^{21} Pas -0.1×10^{21} Pas) and LMV values (1×10^{21} Pas -5×10^{21} Pas). The second solution space includes Earth models with high UMV values (1×10^{21} Pas $- 5 \times 10^{21}$Pas) and intermediate LMV values (5×10^{21} Pas $- 30 \times 10^{21}$Pas). Among the global ice sheet reconstructions, the GLAC3 models exhibit a stronger preference for the second solution space compared to the other background models. A second general result is that all ice models favour solutions with a thinner lithosphere to better reproduce the amplitude of the observed RSL fall (Fig. S4, Appendix).

This is consistent with recent work that indicates relatively high mantle temperatures in southern Greenland compared to the regional average (Ajourlou et al., 2025).

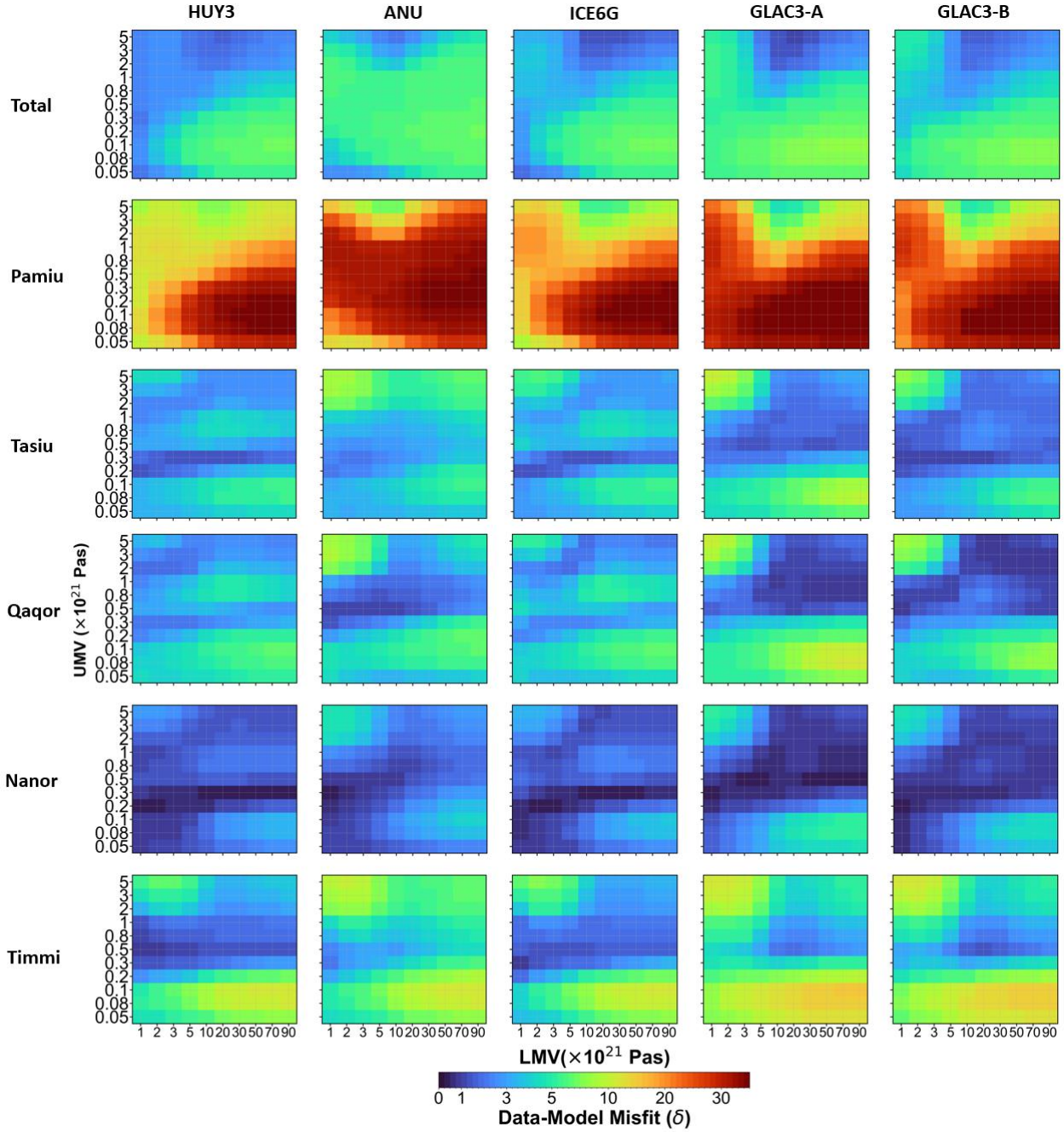

Figure 2.10. Data-model misfit values (δ) as a function of UMV and LMV for an LT value of 71 km. Each column shows results for a different data set (as indicated), and each row shows results for a different ice history model (as indicated).

In Figure 2.11, we provide data-model comparisons for viscosity models from the two solution spaces identified from Fig. 2.10 (top row). In general, the results in Fig. 2.11 show that the model fits to data older than ~8 ka are relatively poor compared to SLIPs in the late Holocene (after ~4 ka). Of the two different earth model parameter sets considered, those with low viscosity values better match the amplitude of RSL fall at most sites and are more compatible with the marine limit. Overall, the data-model fits are disappointing regardless of which optimal viscosity model is chosen. The low viscosity case better matches the marine limit but produces an RSL fall that is too rapid and/or too early, the higher viscosity model produces a rate of RSL fall that is too low.

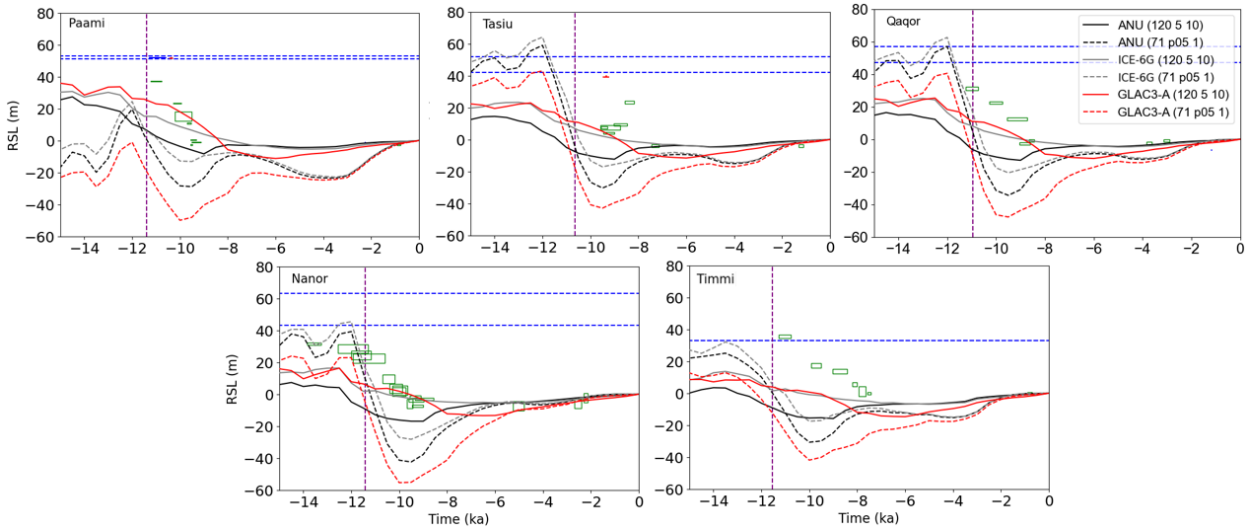

Figure 2.11. RSL curves for earth model parameters from the two solution spaces that result in low misfit values as identified in Fig. 2.9. All curves assume the HUY3 no YD ice model for southern Greenland. Dashed lines are based on the earth model parameters LT = 71 km, UMV = 0.05×10^{21} Pas, LMV = 1×10^{21} Pas and solid lines on LT = 120 km, UMV = 5×10^{21} Pas, LMV = 10×10^{21} Pas. Three different background ice models were used that span the uncertainty associated with this model component (see key). The horizontal dashed blue lines represent the uncertainty in the marine limit, and the dashed vertical purple line are times of final deglaciation at each site (based on the adopted 100 m ice thickness threshold).

Figure 2.10 (rows 2 to 6) show misfit results for individual sites. Comparing results at different sites shows that the quality of fits at Paamiut are poor compared to those at the other sites. This reflects the high precision of the data at this site as well as the relatively poor quality of the data-model fits (evident in Fig 2.11). The results for individual sites also demonstrate that, except for Paamiut, the best fits are obtained with UMV values around $2 - 5 \times 10^{20}$ Pas and relativity low LMV values. This result is most evident when computing misfit results for all sites except Paamiut (Figure 2.12). While there is some variation associated with the adopted background model, the best fits are generally found within this

range of UMV values. The lowest misfit values are obtained with the HUY3 and GLAC3-A models. We show data-model comparisons for these two solutions in Fig. 2.13.

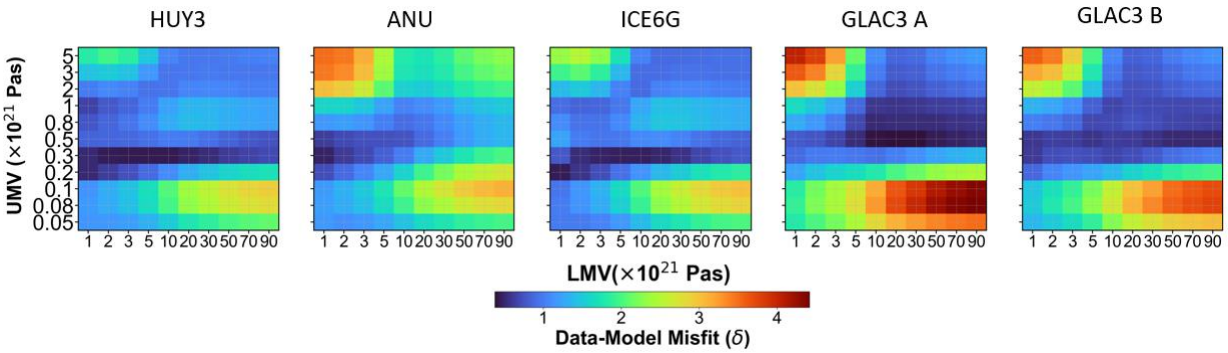

Figure 2.12. Data-model misfit values (δ) for all southern Greenland sites except Paamiut for an LT value of 71 km. Each frame shows results for a different global ice history model (as indicated).

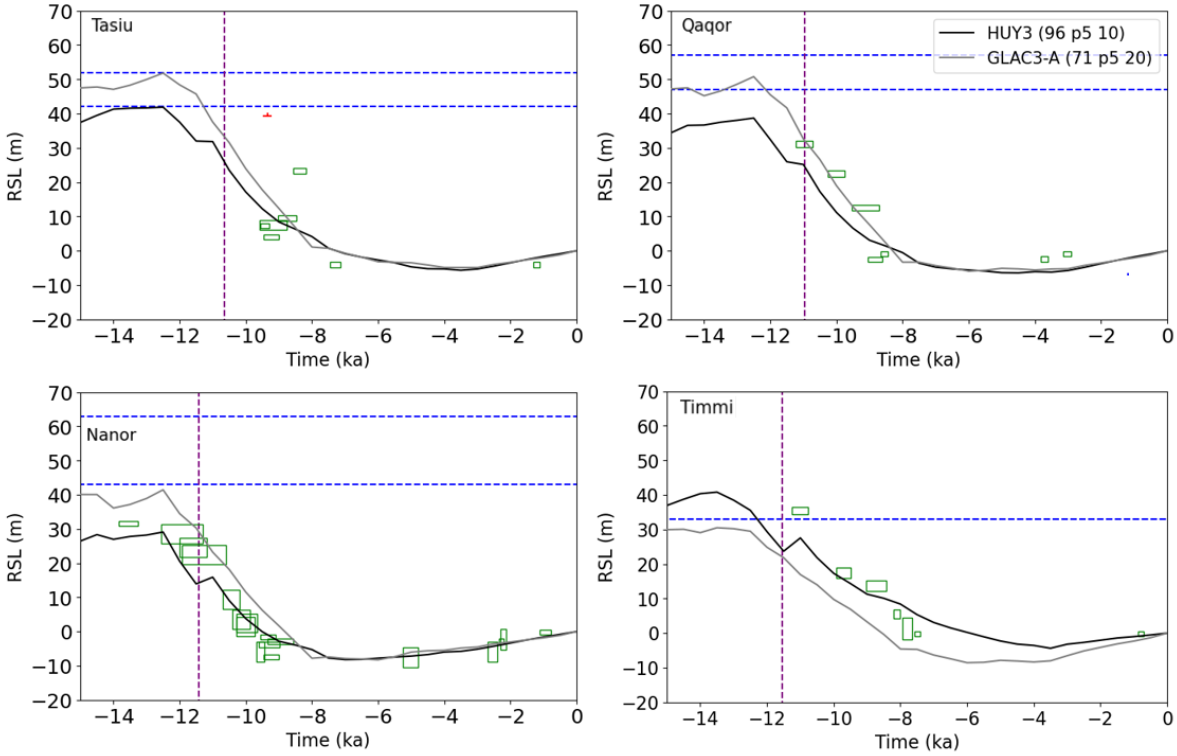

Figure 2.13. RSL curves for the two best scoring data-model misfits. All curves assume the HUY3 no YD ice model for southern Greenland. The black curve is based on the HUY3 background model with earth model parameters: LT = 96 km, UMV = 0.5×10^{21} Pas, LMV = 10×10^{21} Pas, while the gray curve is based on the GLAC3-A ice model with earth model parameters: LT = 71, UMV = 0.5×10^{21} Pas, LMV = 20×10^{21} Pas. The horizontal dashed blue lines represent the uncertainty in the marine limit, and the dashed vertical purple lines are model times of final deglaciation at each site (based on the adopted 100 m ice thickness threshold).

When comparing the results in Figures 2.11 and 2.13, it is clear that the optimal data-model fits are significantly improved when excluding data from Paamiut. When considering both solutions in Fig.

2.13, most of the data are captured (bracketed) by the model curves. The data point at Tasiu (~8.5 ka at ~25m) gives the largest residual. However, this data point is ~10 m higher than other SLIPs of a similar age, indicating that it might be inaccurate. The marine limit constraints are under predicted at most sites, suggesting that an earlier ice retreat might give better results.

2.3.4 3D Earth Modelling

Here, we present a small suite of results based on the revised Greenland ice model presented in Section 2.3.2 and three different global (background) ice models – HUY3, ICE-6G and ANU. The key aspects of the 3D Earth model are the radial viscosity model used as a reference and the scaling parameter (ε) used via Eq. 2.1 to scale lateral temperature variations to viscosity variations (see Section 2.2.2.3). We considered three different ε values (0.02, 0.03 and 0.04 $^{o}C^{-1}$) to determine the sensitivity of our results to this parameter (which governs the strength of the lateral viscosity variations). Our results (Fig. S5, Appendix) indicate that the sensitivity of modelled RSL to this parameter is a few metres or less during the period of sea level fall (post ~13 ka) and so this parameter can be neglected in the remainder of this section. The results that follow adopt the intermediate value of 0.03 $^{o}C^{-1}$ (Latychev et al., 2005).

To examine the influence of lateral structure, we first consider model output of RSL at 10 ka across Greenland (Fig 2.14). The results for a radial earth viscosity model (Fig. 2.14A) show a pattern of RSL that directly reflects the ice mass changes before and after this time. Specifically, the ice loss in peripheral areas contributes to a sea level fall post 10 ka resulting in positive RSL values that exceed 100 m in some regions. The contribution of lateral viscosity structure to RSL at 10 ka acts to diminish RSL predicted using a radial viscosity model (compare Figure 2.14B to 2.14A). The largest signals associated with lateral structure occur in different regions (Fig. 2.14C) and are found in locations where there are large changes in ice loading (i.e., the periphery of Greenland), and where there are considerable variations in lateral earth structure (Fig. 2.4). For example, the large negative signal in southwest Greenland (Fig. 2.14C) is due to the thicker lithosphere and higher viscosities for the 3D earth model resulting in a diminished RSL amplitude at 10ka. (Ajourlou et al., 2025). The influence of lateral structure in southern Greenland is small at 10 ka (< 10 m).

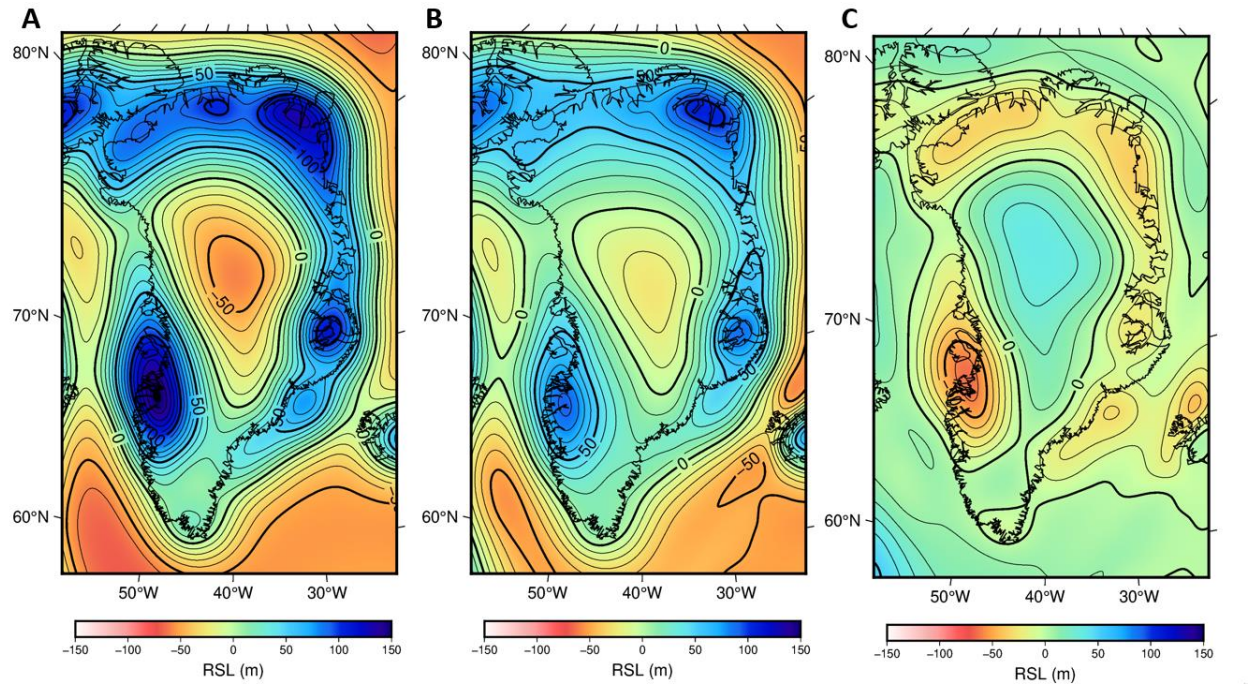

Figure 2.14. Modelled RSL at 10 ka for (A) a radial earth viscosity model with LT = 71 km, UMV = 10^{21} Pas, LMV = 10^{21}, (B) a 3D earth model based on the same radial model as in A and the lateral viscosity structure show in Fig. 2.4. Frame (C) shows the difference between the results in B and A to isolate the influence of the adopted lateral structure.

To examine how the influence of lateral structure on RSL varies in time, we generated model output for the same earth models used in generating Fig. 2.14 (A & B) at the five south Greenland data sites for the revised Greenland ice model (and HUY3 global model) (Fig. 2.15). These results reflect those in Fig. 2.14C in that the influence on lateral structure produces an increase in RSL at Paamiut by several metres at 10 ka but a decrease in RSL at Tasiusaq, Qaqortoq and Nanortalik. Timmiarmiut is located close to the 0 m contour in Fig. 2.14C and so the 1D and 3D model results are very similar at this site – at 10 ka and throughout the Holocene. The difference between the 1D and 3D earth model results is largest, at most sites, in the mid Holocene, with differences exceeding 5 m.

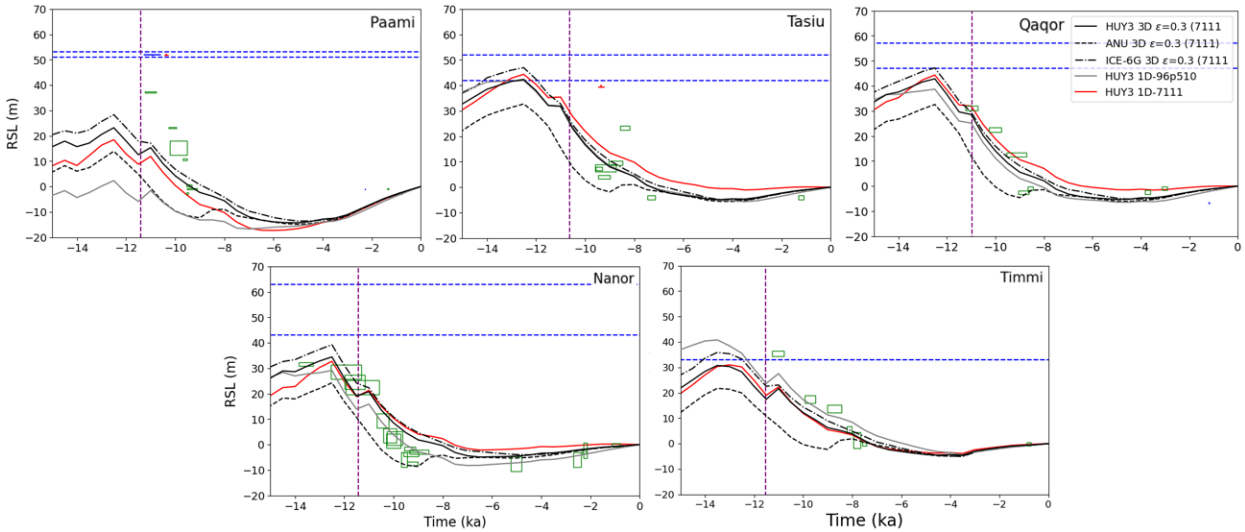

Figure 2.15. Modelled RSL at the five sites in south Greenland. Results are shown for three 3D earth models, each based on the same radial reference model (LT = 71 km, UMV = 10^{21} Pas, LMV = 10^{21}Pas) but a different global (background) ice model (see key). Results are also shown for two 1D earth models, one with the same radial model as the 3D results and one based on the optimal radial model for the case of the HUY3 background model and the exclusion of data at Paamiut (i.e., LT = 96 km, UMV = 0.5×10^{21} Pas, LMV = 10×10^{21} Pas). All curves assume the HUY3 no YD ice model for southern Greenland. The horizontal dashed blue lines represent the uncertainty in the marine limit, and the dashed vertical purple lines are model times of final deglaciation at each site (based on the adopted 100 m ice thickness threshold).

Since the inclusion of lateral structure has a relatively modest influence on modelled RSL in southern Greenland, the influence on the data model fits is minor. For example, while adding lateral structure does improve the data-model fits at Paamiut, since it elevates the RSL curve relative to the 1D case, the data remain poorly fit. For the HUY3 background model, the optimal 1D case (96-p5-10; grey line in Fig. 2.15) gives a misfit of 0.567 compared to 0.618 for the 3D case. For the 3D model runs performed, the misfit values (excluding Paamiut) are 0.619 and 0.636 for ICE-6G and ANU, respectively. Thus, the HUY3 and ICE-6G background models are favoured in this suite of 3D earth modelling results.

Fig 2.16 compares RSL output generated using the best scoring 1D earth model from the misfit analysis (LT = 96 km, UMV = 0.5×10^{21} Pas, LMV = 10×10^{21} Pas) and the optimal 3D earth model from Ajourlou et al. (2025) which adopts the radial model: LT = 71 km, UMV = 10^{21} Pas, LMV = 10^{21}Pas. Across the region, the 3D earth model achieves the lowest misfit 1.885 compared to 3.219 for the best scoring 1D model. The lower score for the 3D model is primarily due to the improved fit at Paamiut where the higher modelled RSL amplitude strongly influences the regional score. When Paamiut is excluded, the best scoring earth model is the 1D earth model (LT = 96 km, UMV = 0.5×10^{21}, LMV = 0.5×10^{21} Pas, LMV = 10×10^{21} Pas) with a misfit of 0.567. Overall, our results indicate that adding lateral structure is significant but does not explain the large misfit at Paamiut.

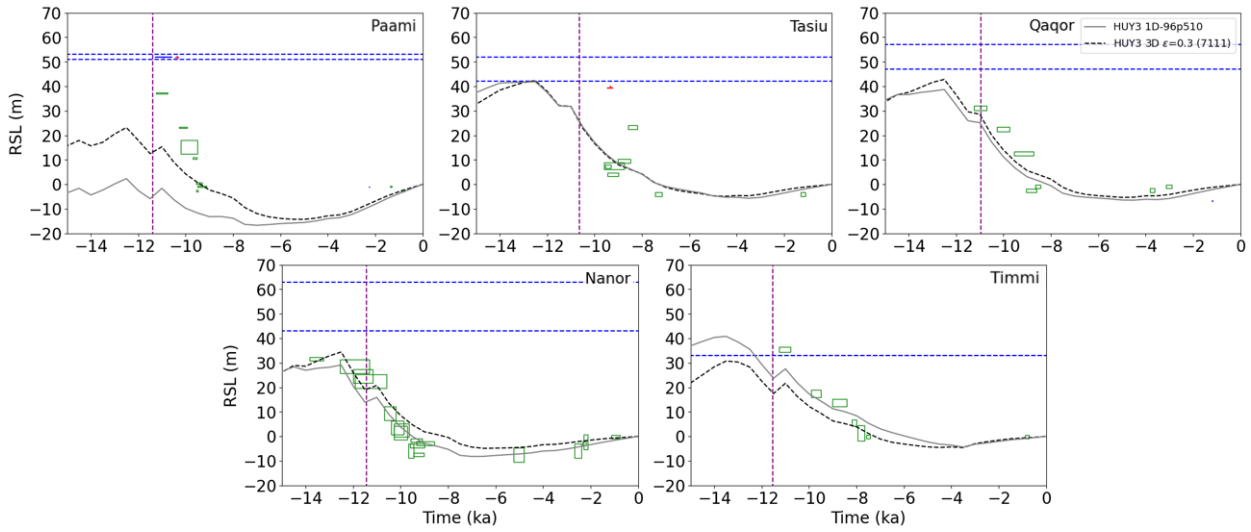

Figure 2.16. Modelled RSL at the five sites in south Greenland. Results are shown for three earth models: the optimal 3D earth model from Ajourlou et al. (2025), which is based on the radial reference model LT = 71 km, UMV = 10^{21} Pas, LMV = 10^{21}Pas and the 1D model that gave the optimal results in our forward modelling analysis: LT = 96 km, UMV = 0.5×10^{21} Pas, LMV = 10×10^{21} Pas. both model curves use the revised southern Greenland chronology and the HUY3 global (background) model (see key). All curves assume the HUY3 no YD ice model for southern Greenland. The horizontal dashed blue lines represent the uncertainty in the marine limit, and the dashed vertical purple lines are model times of final deglaciation at each site (based on the adopted 100 m ice thickness threshold).

2.4 Discussion

A key result of this work includes the explicit consideration of the timing of local model deglaciation such that it is more compatible with the marine limit, SLIPs and cosmogenic constraints (Section 2.3.2). We show that the HUY3 model presented in Lecavalier et al. (2014) is inconsistent with the SLIPs and cosmogenic constraints at most sites. To address this, we developed a revised chronology (Section 2.3.2) which results in improved fits to early Holocene (~12 – 10 ka) RSL observations (Fig.2.17). The RSL predictions based on the revised chronology (Fig 2.17 solid line) produces quality data-model fits at most sites. Paamiut is the clear exception, with neither model getting close to the amplitude or rate of RSL fall at this site.

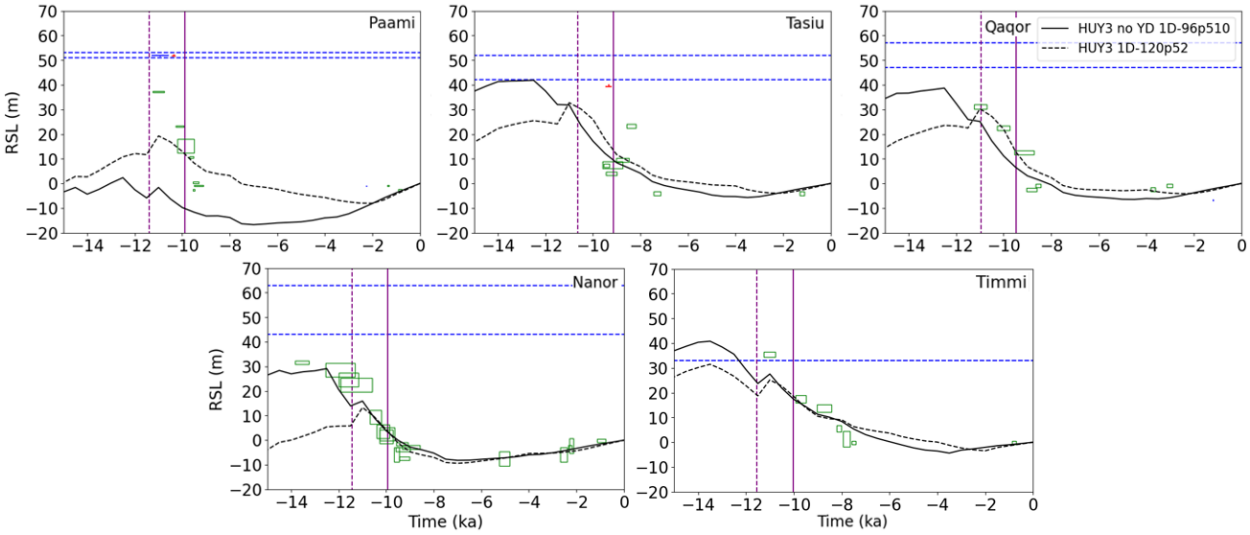

Figure 2.17. Modelled RSL at the five sites in south Greenland. Results are shown for the original HUY3 model with the optimal earth model based on fits to a Greenland-wide RSL data set (Lecavalier et al., 2014; LT = 120 km, UMV = 0.5×10^{21} Pas, LMV = 2×10^{21}Pas) and the optimal parameters from this analysis: LT = 96 km, UMV = 0.5×10^{21} Pas, LMV = 10×10^{21} Pas, using the revised HUY3 chronology (see key). The horizontal dashed blue lines represent the uncertainty in the marine limit, and the dashed vertical purple lines are model times of final deglaciation at each site (based on the adopted 100 m ice thickness threshold) for the HUY3 (solid) and HUY3 no YD models (dashed).

Our results indicate that the poor fits at Paamiut are likely related to the ice model history. Specifically, Figure 2.11 indicates that thicker ice and a later deglaciation would result in improved data-model fits. The poor fits may also be influenced by the location of Paamiut within a fjord. As suggested by Funder et al. (2021), while local coastal areas became ice free, ice may have persisted within major troughs. These more complex deglaciation patterns are generally not well captured in the HUY3 model due to limited spatial resolution (20 km).

Regardless of containing some of the most precise and accurate paleo sea level data around Greenland, the quality of data-model fits in this region are some of the poorest in Greenland. The difficulty in fitting the amplitude of RSL data from southern Greenland have led to the hypothesis of glacially-induced faulting during periods of rapid ice loss (with associated tsunami hazard) (Steffen et al., 2020). Our results demonstrate that by changing local ice and earth models quality data-model fits can be obtained at Nanortalik without inducing large scale faulting. This suggest that large-scale faulting near Nanortalik is not required to explain the data. However, we cannot rule out smaller amplitude faulting in the region.

Results from Sections 2.3.1 and 2.3.3 show that it is necessary to consider multiple background ice models when modelling data in southern Greenland. By considering several different global models, we have quantified the uncertainty associated with this GIA model input and can assess weather certain

models are able to match the data better. Fig 2.5 shows that the non-local ice signal can produce substantial variability in southern Greenland RSL and that the variability in RSL is primarily driven by uncertainties in NAIS and AIS volumes. Fig 2.12 further demonstrates that global ice reconstructions HUY3 and GLAC3-A provide the best fits while the ANU model provides the worst fits.

There are two potential avenues of research that would extend and complement the results presented here, and possibly explain the poor fits at Paamiut. The glaciological model used to produce the Greenland component of the original HUY3 ice history is relatively crude and has been superseded by models with improved physics and higher spatial resolution. Future work should consider the application of these models for southern Greenland, where several sites are located within fjords and the topographic complexity is not fully resolved in the HUY3 model. From an earth modelling perspective, recent work has suggested the possibility of a significant transient component for the deformational response (Paxman et al., 2023). Incorporating this time dependent component of the non-elastic response might better capture the RSL response to rapid load changes in the early Holocene.

2.5 Conclusions

Despite containing some of the most precise and accurate paleo sea level data around Greenland, the quality of data-model fits in this region are some of the poorest. Difficulty in fitting the amplitude of RSL data from southern Greenland has led to the hypothesis of glacially-induced faulting during periods of rapid ice loss (with associated tsunami hazard) (Steffen et al., 2020). Our analysis builds on previous GIA modelling efforts in southern Greenland by revisiting the HUY3 model presented in Lecavalier et al. (2014). Specifically, we consider the timing of local model deglaciation such that it is more compatible with the marine limit, SLIPs and cosmogenic constraints - an aspect that has not been explicitly covered in prior studies. We also consider five different global models of ice evolution so that we can quantify the uncertainty associated with this GIA model input and assess whether certain models are able to match the data better. Finally, we evaluate the impact of 3D earth structure on data-model fits to determine if this structure can significantly improve those obtained with a simpler 1D earth model.

Our results demonstrate that plausible variations in the background ice history model result in significant changes to predicted RSL in southern Greenland. This GIA model input is, therefore, an important source of uncertainty in this region. Of the five different global ice reconstructions considered, HUY3 and GLAC3-A provide the best fits while the ANU model provides the worse fits.

Regarding the earth model parameters, our misfit results demonstrate that RSL data from southern Greenland require lower LT and UMV values compared to previous Greenland-wide analyses (e.g., Lecavalier et al., 2014). Our results suggest that LT values of 71-96 km and UMV of 0.3-0.5 × 10^{21} Pas generally provide good fits at most sites. This finding is compatible with a recent study which constrained lateral temperature and viscosity variations across the Greenland region (Ajourlou et al., 2025). This agreement suggests that constraints on LT and UMV are relatively robust for southern Greenland.

Over the ice and earth model parameter sets considered, quality data-model fits were produced for all sites except Paamiut. Results based on a 3D earth model showed a relatively minor improvement at Paamiut. The results for the other sites were similar to those with the 1D model. In general, adding lateral structure made a relatively minor impact to the data model fits across southern Greenland. We conclude that achieving quality fits at Paamiut will require making revisions to the ice history model. The quality data-model fits obtained at Nanortalik suggest that large-scale faulting is not required to fit the data in the area. However, we cannot rule out smaller amplitude faulting in the region.

Chapter 3 Conclusion

Global mean sea level (GMSL) change is an important indicator for assessing changes in the global climate system as it provides an integrated measure of global warming/cooling. Among the contributors to global mean sea level (GMSL) rise, the Greenland ice sheet (GrIS) stands out as both a current and future threat. GrIS ice volume represents approximately 7m of barystatic sea level (Beckmann and Winkelmann, 2023) and the rate of melting is accelerating, with recent values exceeding 1 mm/yr (Otosaka et al., 2023). This sea level threat is paralleled by the influence of Greenland melting on weakening and potential shutdown of the Atlantic Meridional Ocean Circulation (Van Westen et al., 2024). Thus, there is a clear and urgent need to improve future projections of GrIS mass loss. The work presented in this thesis improves our knowledge of ice sheet changes in southern Greenland since ~15 ka. Knowledge of these past changes informs our understanding of how the ice sheet responded to climate warming, which underpins our ability to project future changes in the ice sheet and thus quantify the hazards outlined above.

The work presented here improves paleo RSL data-model fits in southern Greenland during the last deglaciation. Despite containing some of the most precise and accurate paleo sea level, the quality of data-model fits in past work have been some of the poorest in Greenland (Lecavalier et al., 2014; Woodroffe et al., 2014; Milne et al., 2018). This led to the hypothesis of large magnitude, glacially-induced faulting during a period of rapid ice loss around 10,500 years ago (Steffen et al., 2020). Furthermore, Lecavalier et al. (2014) suggested that the large data-model discrepancies are associated with the influence of lateral earth structure and inaccuracy associated with the on non-Greenland component of the ice model.

We improve paleo RSL data-model fits by directly addressing these limitations: (1) performing a sensitivity analysis to identify the contributions from different component signals; (2) defining a suite of non-Greenland (background) ice models to explicitly include this source of model uncertainty; (3) defining a revised chronology for the southern GrIS that is more compatible with the most recent cosmogenic and RSL constraints; and (4) considering the influence of lateral variations in earth structure using a new 3D model determined from a recent joint inversion of regional data sets (Ajourlou et al., 2025).

A primary contribution of this work includes the explicit consideration of the timing of local model deglaciation such that is compatible with the marine limit, SLIPs and cosmogenic constraints. We show that the HUY3 model presented in Lecavalier et al. (2014) is inconsistent with the SLIPs and cosmogenic constraints at most sites. In terms of the non-Greenland component of the ice model, we

demonstrate that it is necessary to consider multiple background ice models when modelling data in southern Greenland. By considering several different global ice models we can quantify the uncertainty associated with this GIA model input and assess whether certain models are able to match the data better. In southern Greenland we show that the non-local ice signal alone produces variability exceeding 20 m of RSL. Of the five global models considered, HUY3 and GLAC3-A provide the best fits while ANU provides the worst fits in the region.

Regarding the earth model parameters, our misfit results demonstrate that RSL data from southern Greenland require lower LT and UMV values compared to those inferred in previous Greenland-wide analyses (e.g., Simpson et al., 2009; Lecavalier et al., 2014). Our results suggest that LT values of 71-96 km and UMV values of 0.3-0.5 $\times 10^{21}$ Pas generally provide good fits at most sites. This finding is compatible with a recent study which constrained lateral temperature and viscosity variations across the Greenland region (Ajourlou et al., 2025), showing that southern Greenland is characterised by temperatures that are higher than the regional average at depths in the upper few hundred kilometers. This agreement suggests that these constraints on LT and UMV are relatively robust for southern Greenland.

An important conclusion of this work is that, by considering the most recent observational constraints and exploring a broader range of model parameters, quality data-model fits can be obtained in southern Greenland without inducing large amplitude faulting (Steffen et al., 2021). However, we cannot rule out smaller amplitude faulting in the region. Further testing of this hypothesis is important given that the projected future deglaciation of the ice sheet would act to increase the likelihood of faulting in this region (Steffen et al., 2020).

For the ice and earth model parameter sets considered, quality data-model fits were produced for all sites except Paamiut. Results based on a 3D earth model showed relatively minor improvements at Paamiut and hence, achieving quality fits at this site will likely require making revisions to the glaciological model. There are two potential avenues of research that would extend and complement the results presented here, and possibly explain the poor fits at Paamiut. The glaciological model used to produce the Greenland component of the original HUY3 ice history is relatively crude and has been superseded by models with improved physics and higher spatial resolution. Future work should consider the application of these models for southern Greenland, where several sites are located within fjords and the topographic complexity is not fully resolved in the HUY3 model. In addition, we highlight the importance of considering multiple background models and the uncertainty associated with this model input. Future work should incorporate a broader suite of regional glaciological reconstructions to assess the impact of different ice model parameter choices and input climate forcing on modelled RSL in southern Greenland. From an earth modelling perspective, recent work has suggested the possibility of a

significant transient component for the deformational response (Paxman et al., 2023). Incorporating this time dependent component of the non-elastic component of deformation might better capture the RSL response to rapid load changes in the early Holocene (which are particularly evident at Paamiut).

Some results obtained as part of this research project have not been included in this thesis. We have considered more than 15 new glaciological models from a subset GLAC3 simulations provided by Lev Tarasov (Figure 3.1). These 15 models are a subset of many thousands of simulations that produced the best fits to ice extent and RSL data in Greenland. Despite this, it is clear from Fig. 3.1 that these simulations, based on a state-of-the-art glaciological model, underestimate the RSL amplitude in southern Greenland (similar results are obtained at other sites). Since these simulations are based on a large range

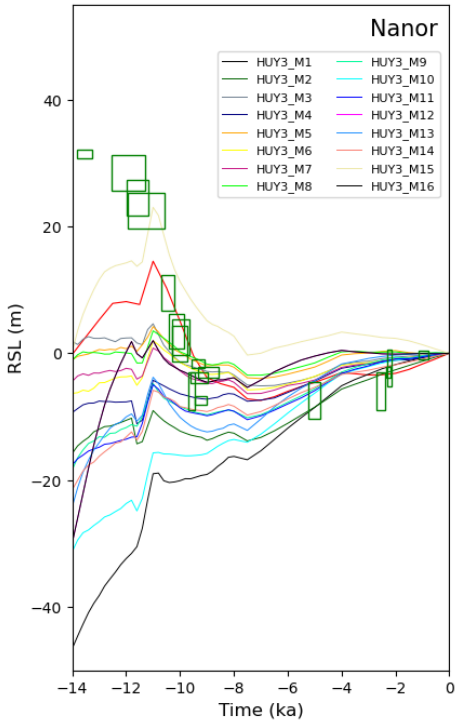

Figure 3.1. Modelled RSL at Nanortalik for all the 15 GLAC3 Greenland ice models with the HUY3 (background) model. The different viscosity models are provided in Table. S1 (Appendix).

of earth model parameters (that encompass the optimal values found in this study), we infer that the poor fits reflect an underestimate in the amount of ice thinning. Further work is necessary to determine which aspects of the glaciological model should be revised to increase the ice thickness.

References

Ajourlou, P., Milne, G. A., Love, R., Afonso, J. C., Salajegheh, F., Latychev, K., Kjeldsen, K. K., Lepipas, A., Martos, Y. M., & Woodroffe, S. A. (2025). Upper mantle temperatures illuminate the Iceland hotspot track and understanding of ice–earth interactions in Greenland. Proceedings of the National Academy of Sciences, 122(50). https://doi.org/10.1073/pnas.2504752122

Ballesteros, C., Lincke, D., Nicholls, R. J., Heslop, J., Hinkel, J., Malagón-Santos, V., & Slangen, A. B. (2025). Migration, land loss and costs to 2100 due to coastal flooding under the IPCC AR6 sea-level rise scenarios and plausible adaptation choices. Frontiers in Marine Science, 12. https://doi.org/10.3389/fmars.2025.1505633

Beckmann, J., & Winkelmann, R. (2023). Effects of extreme melt events on ice flow and sea level rise of the Greenland Ice Sheet. The Cryosphere, 17(7), 3083–3099. https://doi.org/10.5194/tc-17-3083-2023

Bennike, O., & Jepsen, Hans. F. (2000). A new integalacial sequence from Washington Land, Northern Greenland. Polar Research, 19(2), 267–270. https://doi.org/10.3402/polar.v19i2.6551

Dziewonski, A. M., & Anderson, D. L. (1981). Preliminary reference earth model. Physics of the Earth and Planetary Interiors, 25(4), 297–356. https://doi.org/10.1016/0031-9201(81)90046-7

Elsner, J. B. (2006). Evidence in support of the Climate Change–Atlantic hurricane hypothesis. Geophysical Research Letters, 33(16). https://doi.org/10.1029/2006gl026869

Farrell, W. E., & Clark, J. A. (2007). On postglacial sea level. Geophysical Journal of the Royal Astronomical Society, 46(3), 647–667. https://doi.org/10.1111/j.1365-246x.1976.tb01252.x\

Fleming, K., & Lambeck, K. (2004). Constraints on the Greenland ice sheet since the last glacial maximum from sea-level observations and glacial-rebound models. Quaternary Science Reviews, 23(9–10), 1053–1077. https://doi.org/10.1016/j.quascirev.2003.11.001

Funder, S., Kjeldsen, K. K., Kjær, K. H., & Ó Cofaigh, C. (2011). The Greenland Ice Sheet during the past 300,000 years: A Review. Developments in Quaternary Sciences, 699–713. https://doi.org/10.1016/b978-0-444-53447-7.00050-7

Funder, S., Sørensen, A. H., Larsen, N. K., Bjørk, A. A., Briner, J. P., Olsen, J., Schomacker, A., Levy, L. B., & Kjær, K. H. (2021). Younger Dryas ice margin retreat in Greenland: New evidence from Southwestern Greenland. Climate of the Past, 17(2), 587–601. https://doi.org/10.5194/cp-17-587-2021

Glueder, A., Mix, A. C., Milne, G. A., Reilly, B. T., Clark, J., Jakobsson, M., Mayer, L., Fallon, S. J., Southon, J., Padman, J., Ross, A., Cronin, T., & McKay, J. L. (2022). Calibrated relative sea levels constrain isostatic adjustment and ice history in Northwest Greenland. Quaternary Science Reviews, 293, 107700. https://doi.org/10.1016/j.quascirev.2022.107700

Gowan, E. J. (2023). Paleo sea-level indicators and proxies from Greenland in the GAPSLIP database and comparison with modelled sea level from the paleomist ice-sheet reconstruction. GEUS Bulletin, 53. https://doi.org/10.34194/geusb.v53.8355

Hauer, M. E., Hardy, D., Kulp, S. A., Mueller, V., Wrathall, D. J., & Clark, P. U. (2021). Assessing population exposure to coastal flooding due to sea level rise. Nature Communications, 12(1). https://doi.org/10.1038/s41467-021-27260-1

Kendall, R. A., Mitrovica, J. X., & Milne, G. A. (2005). On post-glacial Sea Level - II. numerical formulation and comparative results on spherically symmetric models. Geophysical Journal International, 161(3), 679–706. https://doi.org/10.1111/j.1365-246x.2005.02553.x

Khan, N. S., Horton, B. P., Engelhart, S., Rovere, A., Vacchi, M., Ashe, E. L., Törnqvist, T. E., Dutton, A., Hijma, M. P., & Shennan, I. (2019). Inception of a global atlas of sea levels since the last glacial maximum. Quaternary Science Reviews, 220, 359–371. https://doi.org/10.1016/j.quascirev.2019.07.016

Khan, S. A., Sasgen, I., Bevis, M., van Dam, T., Bamber, J. L., Wahr, J., Willis, M., Kjær, K. H., Wouters, B., Helm, V., Csatho, B., Fleming, K., Bjørk, A. A., Aschwanden, A., Knudsen, P., & Munneke, P. K. (2016). Geodetic measurements reveal similarities between post–last glacial maximum and present-day mass loss from the Greenland Ice Sheet. Science Advances, 2(9). https://doi.org/10.1126/sciadv.1600931

Lambeck, K., Rouby, H., Purcell, A., Sun, Y., & Sambridge, M. (2014). Sea Level and global ice volumes from the last glacial maximum to the holocene. Proceedings of the National Academy of Sciences, 111(43), 15296–15303. https://doi.org/10.1073/pnas.1411762111

Latychev, K., Mitrovica, J. X., Tromp, J., Tamisiea, M. E., Komatitsch, D., & Christara, C. C. (2005). Glacial isostatic adjustment on 3-D Earth Models: A finite-volume formulation. Geophysical Journal International, 161(2), 421–444. https://doi.org/10.1111/j.1365-246x.2005.02536.x

Lecavalier, B. S., & Tarasov, L. (2025). A history-matching analysis of the Antarctic Ice Sheet since the last interglacial – part 1: Ice sheet evolution. The Cryosphere, 19(2), 919–953. https://doi.org/10.5194/tc-19-919-2025

Lecavalier, B. S., Fisher, D. A., Milne, G. A., Vinther, B. M., Tarasov, L., Huybrechts, P., Lacelle, D., Main, B., Zheng, J., Bourgeois, J., & Dyke, A. S. (2017). High arctic holocene temperature record from the Agassiz Ice Cap and Greenland Ice Sheet Evolution. Proceedings of the National Academy of Sciences, 114(23), 5952–5957. https://doi.org/10.1073/pnas.1616287114

Lecavalier, B. S., Milne, G. A., Simpson, M. J. R., Wake, L., Huybrechts, P., Tarasov, L., Kjeldsen, K. K., Funder, S., Long, A. J., Woodroffe, S., Dyke, A. S., & Larsen, N. K. (2014). A model of Greenland ice sheet deglaciation constrained by observations of relative sea level and ice extent. Quaternary Science Reviews, 102, 54–84. https://doi.org/10.1016/j.quascirev.2014.07.018

Leger, T. P., Clark, C. D., Huynh, C., Jones, S., Ely, J. C., Bradley, S. L., Diemont, C., & Hughes, A. L. (2024). A Greenland-wide empirical reconstruction of paleo ice sheet retreat informed by ice extent markers: Paleogris version 1.0. Climate of the Past, 20(3), 701–755. https://doi.org/10.5194/cp-20-701-2024

Levy, L. B., Larsen, N. K., Knudsen, M. F., Egholm, D. L., Bjørk, A. A., Kjeldsen, K. K., Kelly, M. A., Howley, J. A., Olsen, J., Tikhomirov, D., Zimmerman, S. R. H., & Kjær, K. H. (2020). Multi-phased deglaciation of south and southeast Greenland controlled by climate and topographic setting. Quaternary Science Reviews, 242, 106454. https://doi.org/10.1016/j.quascirev.2020.106454

Long, A. J., Woodroffe, S. A., Milne, G. A., Bryant, C. L., & Wake, L. M. (2010). Relative sea level change in West Greenland during the last millennium. Quaternary Science Reviews, 29(3–4), 367–383. https://doi.org/10.1016/j.quascirev.2009.09.010

Long, A. J., Woodroffe, S. A., Roberts, D. H., & Dawson, S. (2011). Isolation basins, sea-level changes and the holocene history of the Greenland Ice Sheet. Quaternary Science Reviews, 30(27–28), 3748–3768. https://doi.org/10.1016/j.quascirev.2011.10.013

Luetzenburg, G., Ngoepe, N., Farnsworth, W. R., Rosenberg, A., Lewis, E., Brodersen, J., Bennike, O., Siggaard-Andersen, M.-L., Woodroffe, S., Milne, G. A., Kjeldsen, K. K., & Larsen, N. K. (2026). Relative sea-level changes and evidence for a holocene low stand in southern Greenland. Quaternary Science Reviews, 374, 109787. https://doi.org/10.1016/j.quascirev.2025.109787

Milne, G. A., & Mitrovica, J. X. (1998). Postglacial sea-level change on a rotating earth. Geophysical Journal International, 133(1), 1–19. https://doi.org/10.1046/j.1365-246x.1998.1331455.x

Milne, G. A., Latychev, K., Schaeffer, A., Crowley, J. W., Lecavalier, B. S., & Audette, A. (2018). The influence of lateral earth structure on glacial isostatic adjustment in Greenland. Geophysical Journal International, 214(2), 1252–1266. https://doi.org/10.1093/gji/ggy189

Milne, G., & Shennan, I. (2013). Sea Level studies | Isostasy: Glaciation-induced sea-level change. Encyclopedia of Quaternary Science, 452–459. https://doi.org/10.1016/b978-0-444-53643-3.00135-7

Mitrovica, J. X., & Peltier, W. R. (1991). On postglacial geoid subsidence over the equatorial oceans. Journal of Geophysical Research: Solid Earth, 96(B12), 20053–20071. https://doi.org/10.1029/91jb01284

Mitrovica, J. X., & Milne, G. A. (2003). On post-glacial sea level: I. general theory. Geophysical Journal International, 154(2), 253–267. https://doi.org/10.1046/j.1365-246x.2003.01942.x

Mitrovica, Jerry X., Wahr, J., Matsuyama, I., & Paulson, A. (2005). The rotational stability of an ice-age Earth. Geophysical Journal International, 161(2), 491–506. https://doi.org/10.1111/j.1365-246x.2005.02609.x

Fox-Kemper, B., H.T. Hewitt, C. Xiao, G. Aðalgeirsdóttir, S.S. Drijfhout, T.L. Edwards, N.R. Golledge, M. Hemer, R.E. Kopp, G. Krinner, A. Mix, D. Notz, S. Nowicki, I.S. Nurhati, L. Ruiz, J.-B. Sallée, A.B.A. Slangen, and Y. Yu, 2021: Ocean, Cryosphere and Sea Level Change. In Climate Change 2021: The Physical Science Basis. Contribution of Working Group I to the Sixth Assessment Report of the Intergovernmental Panel on Climate Change [Masson-Delmotte, V., P. Zhai, A. Pirani, S.L. Connors, C. Péan, S. Berger, N. Caud, Y. Chen, L. Goldfarb, M.I. Gomis, M. Huang, K. Leitzell, E. Lonnoy, J.B.R. Matthews, T.K. Maycock, T. Waterfield, O. Yelekçi, R. Yu, and B. Zhou (eds.)]. Cambridge University Press, 1211–1362. https://doi.org/10.1017/9781009157896.011

Otosaka, I. N., Shepherd, A., Ivins, E. R., Schlegel, N.-J., Amory, C., van den Broeke, M. R., Horwath, M., Joughin, I., King, M. D., Krinner, G., Nowicki, S., Payne, A. J., Rignot, E., Scambos, T., Simon, K. M., Smith, B. E., Sørensen, L. S., Velicogna, I., Whitehouse, P. L., A, G., Agosta, C., Ahlstrøm, A. P., Blazquez, A., Colgan, W., Engdahl, M. E., Fettweis, X., Forsberg, R., Gallée, H., Gardner, A., Gilbert, L., Gourmelen, N., Groh, A., Gunter, B. C., Harig, C., Helm, V., Khan, S. A., Kittel, C., Konrad, H., Langen, P. L., Lecavalier, B. S., Liang, C.-C., Loomis, B. D., McMillan, M., Melini, D., Mernild, S. H., Mottram, R., Mouginot, J., Nilsson, J., Noël, B., Pattle, M. E., Peltier, W. R., Pie, N., Roca, M., Sasgen, I., Save, H. V., Seo, K.-W., Scheuchl, B., Schrama, E. J. O., Schröder, L., Simonsen, S. B., Slater, T., Spada, G., Sutterley, T. C., Vishwakarma, B. D., van Wessem, J. M., Wiese, D., van der Wal, W., and Wouters, B.: Mass balance of the Greenland and Antarctic ice sheets from 1992 to 2020, Earth Syst. Sci. Data, 15, 1597–1616, https://doi.org/10.5194/essd-15-1597-2023, 2023.Peltier, W. R. (2004). Global glacial isostasy and the surface of the ice-age earth: The ice-5G (VM2) model and Grace. Annual Review of Earth and Planetary Sciences, 32(1), 111–149. https://doi.org/10.1146/annurev.earth.32.082503.144359

Parang, S., Milne, G. A., Tarasov, L., Love, R., Yousefi, M., & Vacchi, M. (2024). Constraining models of glacial isostatic adjustment in eastern North America. Quaternary Science Reviews, 334, 108708. https://doi.org/10.1016/j.quascirev.2024.108708

Paxman, G. J., Lau, H. C., Austermann, J., Holtzman, B. K., & Havlin, C. (2023). Inference of the timescale-dependent apparent viscosity structure in the upper mantle beneath Greenland. AGU Advances, 4(2). https://doi.org/10.1029/2022av000751

Peltier, W. R. (1974). The impulse response of a maxwell Earth. Reviews of Geophysics, 12(4), 649–669. https://doi.org/10.1029/rg012i004p00649

Peltier, W. R., Argus, D. F., & Drummond, R. (2015). Space geodesy constrains ice age terminal deglaciation: The global ice-6g_c (VM5A) model. Journal of Geophysical Research: Solid Earth, 120(1), 450–487. https://doi.org/10.1002/2014jb011176

Simpson, M. J. R., Milne, G. A., Huybrechts, P., & Long, A. J. (2009). Calibrating a glaciological model of the Greenland Ice Sheet from the last glacial maximum to present-day using field observations of relative sea level and ice extent. Quaternary Science Reviews, 28(17–18), 1631–1657. https://doi.org/10.1016/j.quascirev.2009.03.004

Simpson, M. J., Wake, L., Milne, G. A., & Huybrechts, P. (2011). The influence of decadal- to millennial-scale ice mass changes on present-day vertical land motion in Greenland: Implications for the interpretation of GPS observations. Journal of Geophysical Research, 116(B2). https://doi.org/10.1029/2010jb007776

Sinclair, G., Carlson, A. E., Mix, A. C., Lecavalier, B. S., Milne, G., Mathias, A., Buizert, C., & DeConto, R. (2016). Diachronous retreat of the Greenland Ice Sheet during the last deglaciation. Quaternary Science Reviews, 145, 243–258. https://doi.org/10.1016/j.quascirev.2016.05.040

Steffen, R., Steffen, H., Weiss, R., Lecavalier, B. S., Milne, G. A., Woodroffe, S. A., & Bennike, O. (2020). Early Holocene Greenland-ice mass loss likely triggered earthquakes and tsunami. Earth and Planetary Science Letters, 546, 116443. https://doi.org/10.1016/j.epsl.2020.116443

Tarasov, L., & Richard Peltier, W. (2002). Greenland glacial history and local geodynamic consequences. Geophysical Journal International, 150(1), 198–229. https://doi.org/10.1046/j.1365-246x.2002.01702.x

Tarasov, L., Dyke, A. S., Neal, R. M., & Peltier, W. R. (2012). A data-calibrated distribution of deglacial chronologies for the North American ice complex from glaciological modeling. Earth and Planetary Science Letters, 315–316, 30–40. https://doi.org/10.1016/j.epsl.2011.09.010

Van Westen, R. M., Kliphuis, M., & Dijkstra, H. A. (2024). Physics-based early warning signal shows that AMOC is on tipping course. Science Advances, 10(6). https://doi.org/10.1126/sciadv.adk1189

Weidick, A., & Bennike, O. (2007). Quaternary glaciation history and glaciology of Jakobshavn Isbræ and the Disko Bugt Region, West Greenland: A Review. Geological Survey of Denmark and Greenland Bulletin, 14, 1–78. https://doi.org/10.34194/geusb.v14.4985

Whitehouse, P. L. (2018). Glacial isostatic adjustment modelling: Historical Perspectives, recent advances, and Future Directions. Earth Surface Dynamics, 6(2), 401–429. https://doi.org/10.5194/esurf-6-401-2018

Woodroffe, S. A., & Long, A. J. (2010). Reconstructing recent relative sea-level changes in West Greenland: Local diatom-based transfer functions are superior to regional models. Quaternary International, 221(1–2), 91–103. https://doi.org/10.1016/j.quaint.2009.06.005

Woodroffe, S. A., Long, A. J., Lecavalier, B. S., Milne, G. A., & Bryant, C. L. (2014). Using relative sea-level data to constrain the deglacial and holocene history of southern Greenland. Quaternary Science Reviews, 92, 345–356. https://doi.org/10.1016/j.quascirev.2013.09.008

Woodroffe, S. A., Wake, L. M., Kjeldsen, K. K., Barlow, N. L., Long, A. J., & Kjær, K. H. (2023). Missing sea level rise in southeastern Greenland during and since the Little Ice Age. Climate of the Past, 19(8), 1585–1606. https://doi.org/10.5194/cp-19-1585-2023

Appendix

Supplementary Figures

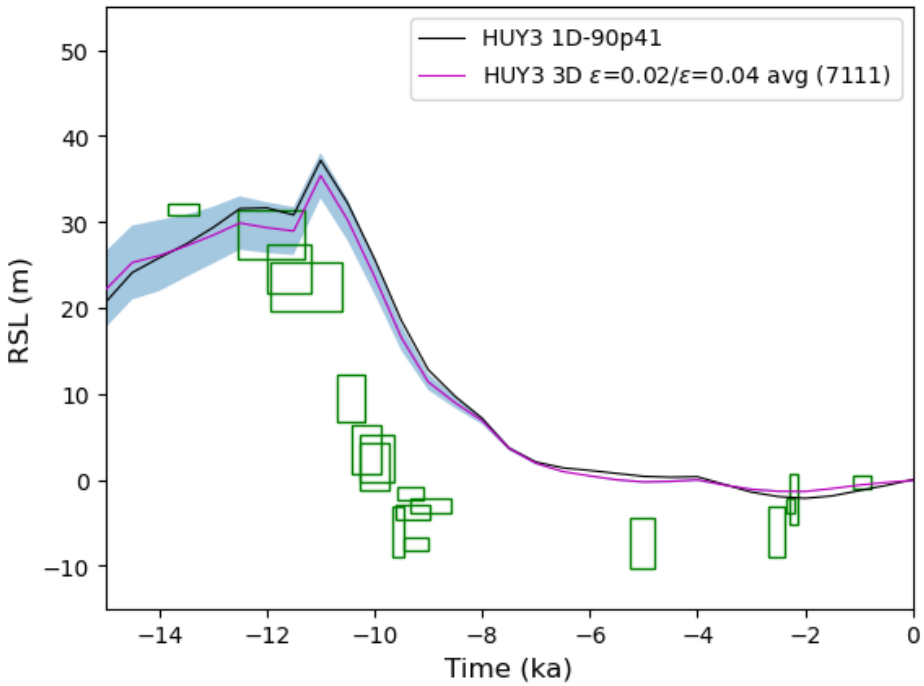

Figure S1. Modelled RSL curves for a 1D earth model of LT = 90 km, UMV = 0.04×10^{21} Pas, LMV = 1×10^{21} Pas (solid black line) and an average of the 3D model results based on ε = 0.02 $^{o}C^{-1}$ and ε = 0.04$^{o}C^{-1}$ (solid pink line). The blue band shows the range defined by the two ε values. All curves in the plot use the HUY3 chronology presented in Lecavalier et al. (2014). Green boxes indicate SLIPs reconstructed at this site (with box dimensions showing 2σ uncertainty in RSL and age).

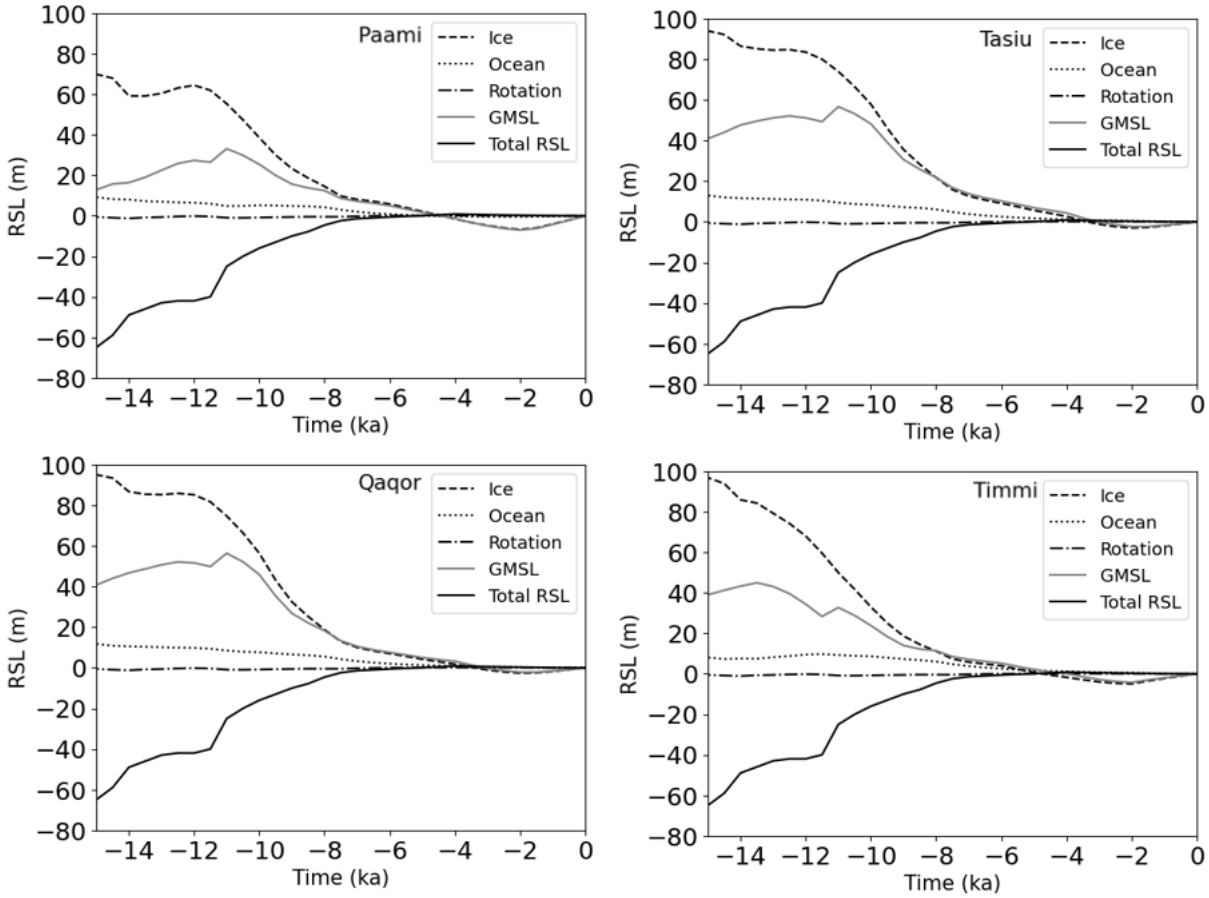

Figure S2. Contributions from different component signals (see key) to RSL for the period 14 – 0 ka. Results are based on the HUY3 ice model and earth model parameters LT = 90 km, UMV = 0.4×10^{21} Pas, LMV = 1×10^{21} Pas.

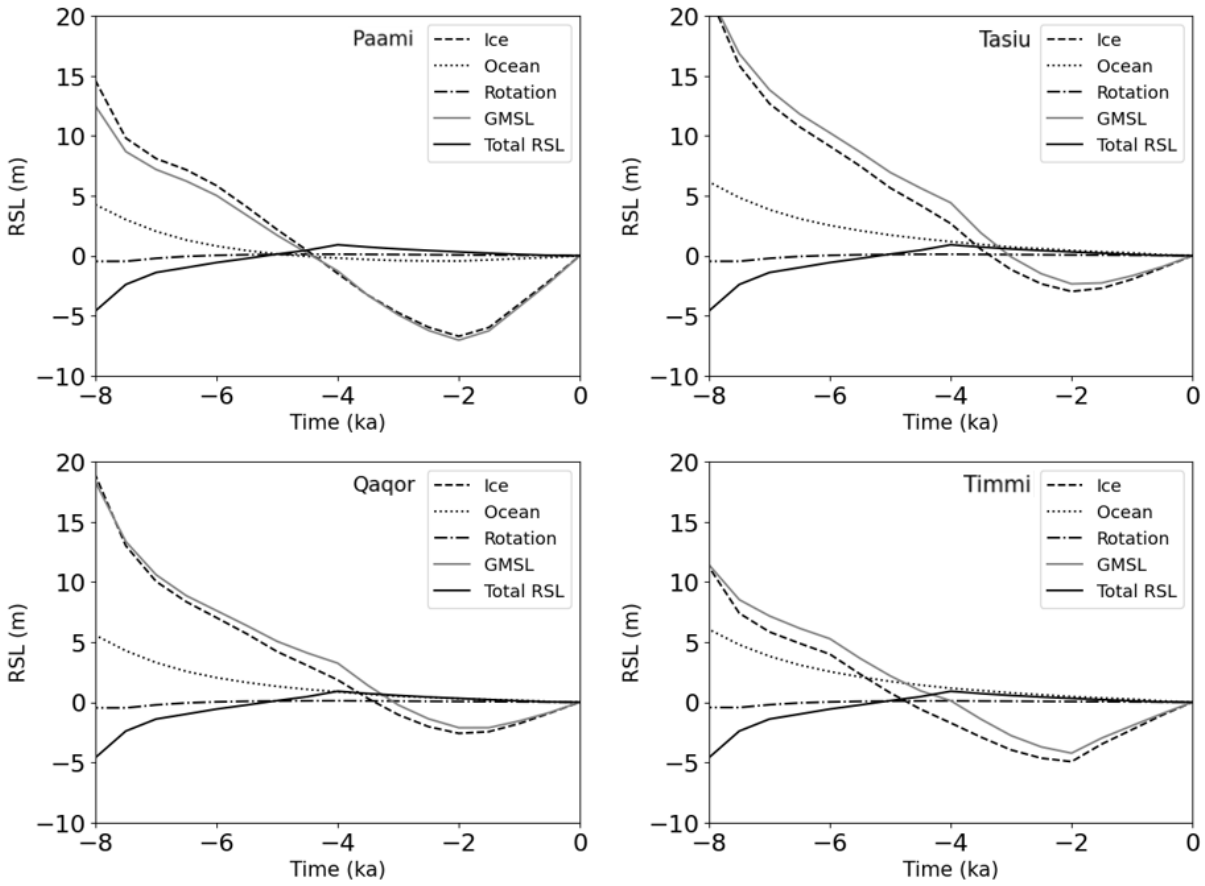

Figure S3. Contributions from different component signals (see key) to RSL for the period 8 – 0 ka. Results are based on the HUY3 ice model and earth model parameters LT = 90 km, UMV = 0.4×10^{21} Pas, LMV = 1×10^{21} Pas.

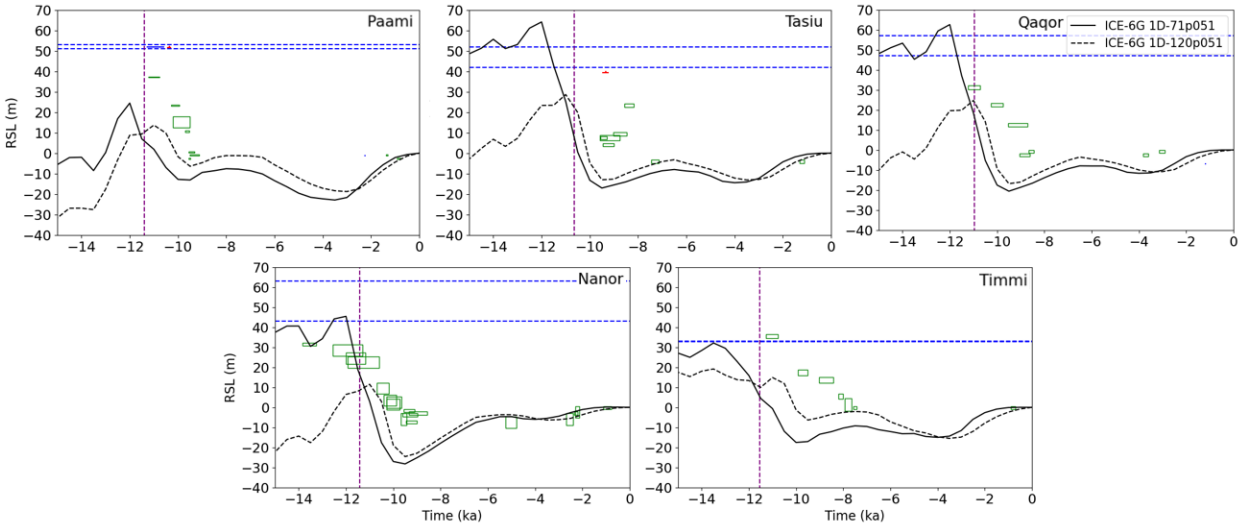

Figure S4. RSL curves using the HUY3 no YD local ice sheet model and the ICE-6G background (global) model. Results are shown for two 1D earth models LT = 71 km, UMV = 0.5×10^{21} Pas, LMV = 1×10^{21}Pas) and LT = 120 km, UMV = 0.5×10^{21} Pas, LMV = 1×10^{21}Pas) (see key). The horizontal dashed blue lines represent the uncertainty in the marine limit, and the dashed purple vertical lines show modelled ice-free conditions (when ice thickness is below 100 m).

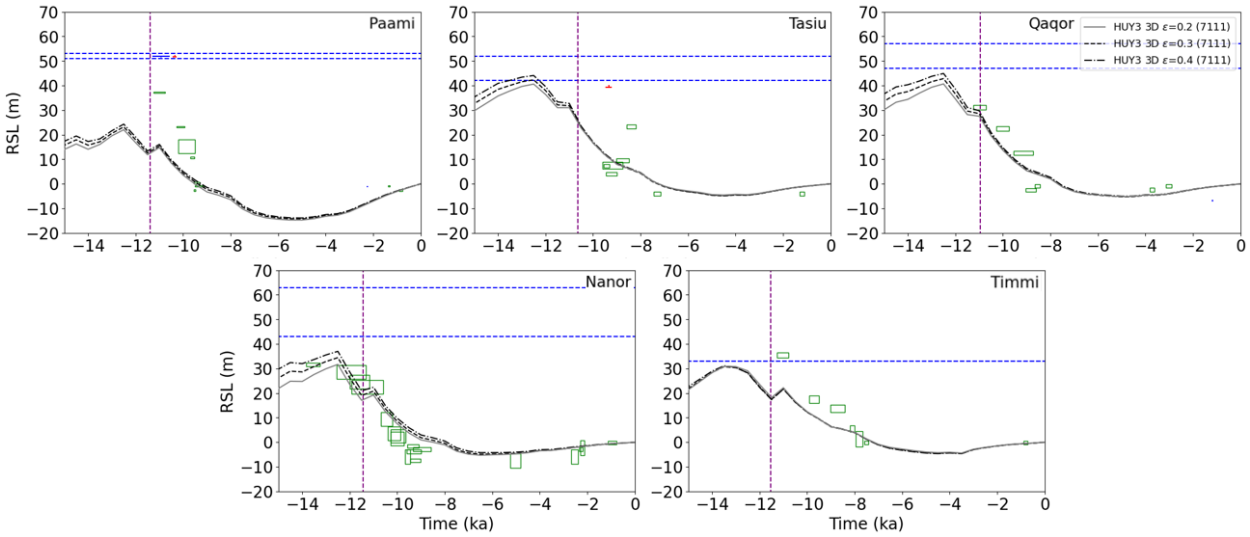

Figure S5. RSL curves using the HUY3 no YD ice sheet model. Results are shown for three 3D earth models, each based on the same radial reference model (LT = 71 km, UMV = 10^{21} Pas, LMV = 10^{21}Pas) for ε = 0.02, 0.03 and 0.04 $^{o}C^{-1}$ (see key). The horizontal dashed blue lines represent the uncertainty in the marine limit, and the dashed purple vertical lines show modelled ice-free conditions (when ice thickness is below 100 m).

Ice loading history	Ideal 1D Earth model parameters		
	LT (km)	UMV ($\times 10^{21}$ Pas)	LMV ($\times 10^{21}$ Pas)
HUY3	120	0.5	2
M1 (42372G)	96	0.5	2
M2 (43096G)	120	2	10
M3 (43145G)	71	5	30
M4 (43396G)	146	1	20
M5 (44408G)	46	5	50
M6 (44612G)	46	3	30
M7 (44651G)	120	2	20
M8 (44923G)	146	3	30
M9 (45753G)	71	2	10
M10 (45902G)	46	0.8	10
M11 (46175G)	46	2	50
M12 (46321G)	46	0.1	1
M13 (46371G)	71	0.1	1
M14 (46376G)	71	0.5	5
M15 (46441G)	46	0.1	1

Table S1. List of the subset of 15 GLAC3 ice model reconstructions with their partnering 1D Earth viscosity models. HUY3 model is also included.